Proteasome-dependent Orc6 removal from chromatin upon S-phase entry safeguards against MCM reloading and tetraploidy

running title: Orc6 removal limits MCM reloading

Yoko Hayashi-Takanaka[1,2,*], Ichiro Hiratani[2], Tokuko Haraguchi[1] and Yasushi Hiraoka[1*]

[1] Graduate School of Frontier Biosciences, Osaka University, 1-3 Yamadaoka, Suita 565-0871, Japan

[2] RIKEN Center for Biosystems Dynamics Research, 2-2-3 Minatojima-minamimachi, Chuo-ku, Kobe 650-0047 Japan

[*]Correspondence should be addressed to:

Yoko Hayashi-Takanaka

RIKEN Center for Biosystems Dynamics Research, 2-2-3 Minatojima-minamimachi, Chuo-ku, Kobe 650-0047 Japan

E-mail: yoko.hayashi.yr@riken.jp

or

Yasushi Hiraoka

Graduate School of Frontier Biosciences, Osaka University, 1-3, Yamadaoka, Suita, 565-0871, Japan

E-mail: hiraoka@fbs.osaka-u.ac.jp

Abstract

DNA replication is tightly regulated to occur only once per cell cycle, as untimely re-initiation can lead to aneuploidy, which is associated with early senescence and cancer. The pre-replication complex (comprising Orc1-6, Cdc6, Cdt1, and MCM) is essential for the initiation of DNA replication, but the dynamics and function of Orc6 during the cell cycle remain elusive. Here, we demonstrate that Orc6 associates with chromatin during G1-phase and dissociates upon S-phase entry. The dissociation of Orc6 from chromatin is dependent on proteasome activity, and inhibition of the proteasome leads to the accumulation of chromatin-bound Orc6, which promotes abnormal MCM loading after S-phase entry without undergoing mitosis in human immortalized hTERT-RPE1 cells. Following release from proteasome inhibition, cells with elevated levels of chromatin-bound Orc6 and MCM proceed to the next replication phase as tetraploid cells. Our findings suggest that the proteasome-dependent dissociation of Orc6 after DNA replication is critical for preventing inappropriate MCM reloading and tetraploid formation.

Keywords (3-6 words)

Orc6; DNA replication; MCM; proteasome; tetraploid; single-cell plot analysis

Introduction

Genomic DNA replication is fundamental to the proliferation of living organisms. In eukaryotes, this process is tightly regulated to ensure that all chromosomes replicate only once per cell cycle. Disruptions in this regulation can result in abnormal DNA replication, leading to genomic instability, which may promote senescence or oncogenesis (Thakur et al., 2022).

DNA replication begins with the assembly of pre-replication complexes (pre-RCs) at replication origins during G1 phase (Hu and Stillman, 2023). The pre-RC consists of four key components: the origin recognition complex (ORC), minichromosome maintenance (MCM) complex, Cdc6, and Cdt1. MCM, a replicative helicase, is composed of Mcm2–7 subunits (Bell and Botchan, 2013; Deegan and Diffley, 2016; Ishimi, 2018), while Cdc6 and Cdt1 facilitate the recruitment of MCM to chromatin. Upon entry into S-phase, the pre-RC disassembles. Aberrant loading of pre-RCs onto chromatin after the S-phase initiation can trigger DNA re-replication without mitosis (Vassilev and DePamphilis, 2017; Limas and Cook, 2019), underscoring the need for tight regulation of Cdt1 and Cdc6 levels by proteasome degradation through E3 ubiquitin ligases to prevent pre-RC formation beyond G1 phase (Nishitani et al., 2006; Walter et al., 2016).

The ORC is a six-subunit complex (Orc1–6), which binds chromatin to mark replication origins for pre-RC assembly during G1 phase (Bell and Labib, 2016; Ganier et al., 2019; Hu and Stillman, 2023). While Orc2–5 remain chromatin-bound throughout the cell cycle, Orc1 dissociates from chromatin after S-phase entry via ubiquitin-mediated proteolysis (Li and DePamphilis, 2002; Méndez et al., 2002; Tatsumi et al., 2003; Coulombe et al., 2019). Orc1–5 share structural similarities, whereas Orc6 is more similar

69 to TFIIB (Duncker et al., 2009; Liu et al., 2011; Feng et al., 2021), distinguishing it
70 functionally from other ORCs. Orc6 can bind DNA independently of Orc1-5 (Xu et al.,
71 2020) and has roles in chromosome segregation and cytokinesis (Prasanth et al., 2002;
72 Chesnokov et al., 2003; Semple et al., 2006; Balasov et al., 2009; Bernal and
73 Venkitaraman, 2011). Recent studies suggest additional functions for Orc6, including its
74 involvement in replication fork progression, ATR activation, and mismatch repair (Lin et
75 al., 2022). However, the specific role of human Orc6 in the cell cycle remains largely
76 unexplored.

77 Proteasomes are the primary machinery for protein degradation in cells. Reduced
78 proteasome activity is observed in replicative senescent cells (Sabath et al., 2020) and
79 inhibiting proteasomes induces cellular senescence in normal human fibroblasts
80 (Chondrogianni & Gonos, 2004; Chondrogianni et al., 2003; Torres et al., 2006; Ukekawa
81 et al., 2004). Senescent cells, which bypass mitosis, exhibit chromatin-bound pre-RCs,
82 suggesting a predisposition to enter S-phase as tetraploid cells (Johmura et al., 2014;
83 Panopoulos et al., 2014; Zeng et al., 2023). However, it remains unclear whether reduced
84 proteasome activity in cellular senescence is involved in pre-RC formation.

85 In this study, we explored the dynamics of Orc6 during the cell cycle in human
86 cells using multicolor immunofluorescence-based single-cell plot analysis (hereafter
87 referred to as "single-cell plot analysis"). This method allows for the quantitative
88 measurements of Orc6 levels in individual cells from fluorescence microscopy images,
89 eliminating the need for cell synchronization (Hayashi-Takanaka et al., 2020; Hayashi-
90 Takanaka et al., 2021). Our findings suggest that the regulation of Orc6 localization
91 throughout the cell cycle is crucial for proper pre-RC formation, and its dysregulation can
92 lead to replication as tetraploid cells.

Results

Dissociation of Orc6 from chromatin during S-phase

To quantify chromatin-bound Orc6 in individual human cells, we performed single-cell plot analysis using fluorescence microscopy to measure multiple intracellular components in each cell (Hayashi-Takanaka et al., 2020; Hayashi-Takanaka et al., 2021). An asynchronous population of hTERT-RPE1 cells was fixed using two different methods: "direct fixation" and "pre-extraction" (Fig. 1A). The direct fixation method detects whole nuclear proteins, while the pre-extraction method detects only the chromatin-bound fraction (Hayashi-Takanaka et al., 2021). The fixed cells were stained with Hoechst 33342 (a DNA indicator, referred to as "Hoechst"), EdU (an S-phase marker), and an anti-Orc6 antibody (Fig. 1A). The same cells were also stained with an anti-Orc2 antibody to detect the behavior of Orc2–5 subunits on chromatin throughout the cell cycle. The specificity of these antibodies was validated by immunostaining as shown in Fig. S1.

Fluorescence imaging revealed that Orc6 staining was relatively uniform in the cell population when using the direct fixation method but showed variability among the cells prepared by the pre-extraction method (compare upper and lower panels for Orc6 in Fig. 1A). In contrast, Orc2 staining appeared punctate and remained consistent across all cells in both methods (right panels, Fig. 1A). Single-cell plot analysis was performed based on these images: the DNA content was determined by Hoechst intensity normalized from 1 to 2, and the normalized intensities of EdU, Orc6, and Orc2 were plotted against the DNA content, where each dot represents a single cell (Fig. 1B). EdU-positive S-phase cells (>-2 on the $\log_2$ scale), marked as orange dots in the EdU panels (left panels, Fig. 1B), are also shown as orange dots in both the Orc6 and Orc2

117 panels (middle and right panels, Fig. 1B). In the direct fixation method, the whole
118 fraction of Orc6 levels remained relatively constant, ranging from −1 to 1 on the $\log_2$
119 scale throughout the cell cycle (upper middle panel, Fig. 1B). However, using the pre-
120 extraction method, chromatin-bound Orc6 levels were high during G1-phase, dropped
121 immediately after S-phase entry, and stayed low through S- and G2-phases (lower
122 middle panel, Fig. 1B). Orc2 levels remained relatively constant during the G1/S
123 transition and showed minimal changes during the S-phase in both fixation methods
124 (right panels, Fig. 1B). These results indicate that Orc6, but not Orc2, dissociates from
125 chromatin during S-phase in hTERT-RPE1 cells.
126 To determine if Orc6 dissociation occurs in other cell types, we analyzed
127 changes in chromatin-bound Orc6 levels during the cell cycle in cancer cell lines (HeLa
128 and U2OS cells) and normal fibroblast cells (IMR90 cells) using the pre-extraction
129 method (Fig. S2A). The reduction in Orc6 levels during the G1- to S-phase transition
130 was less pronounced in cancer cell lines (HeLa and U2OS cells, Fig. S2B) compared to
131 normal cell lines (IMR90 and hTERT-RPE1 cells, Fig. S2B). This suggests that the
132 regulation of chromatin-bound Orc6 levels during the cell cycle may differ between
133 normal and cancer cells, or among different cell types.
134
135 **Involvement of the proteasome in Orc6 dissociation from chromatin**
136 Since the levels of Cdt1, a component of the pre-RC, are regulated by proteasome
137 activity, we examined whether Orc6 is also a target for proteasome regulation using the
138 proteasome inhibitor MG132. hTERT-RPE1 cells were treated with 20 μM MG132 for
139 varying durations (1, 2, and 4 h), fixed using the two different fixation methods, and
140 stained with Hoechst and an anti-Orc6 antibody. The same cells were co-stained with

141 anti-Cdt1 and anti-Orc2 antibodies as controls for proteasome degradation (Fig. 2A).
142 Single-cell plot analysis revealed that Orc6 levels in the whole fraction (obtained by the
143 direct-fixation method) remained relatively unchanged for up to 2 h of MG132
144 treatment (blue dots, left panels in Fig. 2A). However, in the chromatin-bound fraction
145 (obtained by the pre-extraction method), Orc6 was predominantly bound to chromatin
146 during G1-phase and dissociated after S-phase entry under control conditions (DMSO
147 treatment). Upon the treatment with MG132 for 1 h, the decrease in Orc6 levels at the
148 G1- to S-phase transition was less pronounced (blue dots, right panels in Fig. 2A). After
149 2 h of MG132 treatment, Orc6 remained bound to chromatin after the S-phase, similar
150 to its levels in G1-phase.
151 Cdt1 levels increased in cells progressing through S and G2 phases after 1 h
152 of treatment and continued to increase with extended treatment in both fixation methods
153 (orange dots, Fig. 2A), indicating that proteasome degradation was functioning
154 normally under these experimental conditions. Orc2 levels remained relatively
155 unchanged for up to 4 h in the direct fixation method (green dots, left panels in Fig.
156 2A), and slightly increased after 4 h in the pre-extraction method (green dots, right
157 panels in Fig. 2A). These results suggest that Orc6, and to a lesser extent Orc2, is not
158 degraded by the proteasome during the S and G2 phases but instead dissociates from
159 chromatin via proteasome activity.
160 To compare the increase in Orc6 levels during the S-phase due to MG132
161 treatment with that of Cdt1 and Orc2, S-phase cells were selected based on Hoechst
162 intensity (1.1< Hoechst <1.75) from the single-cell plot analysis (Fig. 2A), and then the
163 fluorescence intensity was plotted during the time course of MG132 treatment (each dot
164 represents a single cell, Fig. 2B and S3D, E). The results showed little to no increase in

165 Orc6 and Orc2 levels in the whole fraction after up to 4 h of treatment (1–2-fold; whole
166 fraction, Fig. 2B), while a large increase in Cdt1 levels was observed with increasing
167 duration of MG132 treatment (up to 8-fold; whole fraction, Fig. 2B). In the chromatin-
168 bound fraction, Orc6 levels in S-phase cells showed a substantial increase with
169 prolonged MG132 treatment (up to 8-fold; chromatin-bound fraction, Fig. 2B), while
170 those in G1- and G2-phase cells increased mildly (up to 4-fold; chromatin-bound
171 fraction, Fig. S3D, E). The increase in chromatin-bound Cdt1 and Orc2 levels was
172 smaller compared to Orc6 (up to 5-fold and 3-fold, respectively; chromatin-bound
173 fraction, Fig. 2B). Orc6 binding to chromatin was not affected by the depletion of either
174 Orc1 or Orc2 (Fig. S3A-C), suggesting that the MG132-induced increase in chromatin-
175 bound Orc6 was independent of the presence of Orc1 or Orc2. Similar analyses for G1
176 and G2 phases showed that the changes in chromatin-bound Orc6 due to MG132 were
177 less pronounced than in S-phase (Fig. S3D, E).
178 To further confirm these results, we examined Orc6 protein levels in whole-cell
179 lysates and chromatin fractions obtained via sucrose cushion fractionation (Fig. 2C).
180 Cells were treated with 20 μM MG132 for varying durations (1, 2, and 4 h), and Orc6
181 levels were analyzed in whole-cell lysates and chromatin fractions by western blotting
182 (Fig. 2D). Orc6 levels in whole-cell lysates remained unchanged throughout MG132
183 treatment (whole, top row, Fig. 2D). In contrast, in the chromatin fractions, Orc6 levels
184 increased approximately 3-fold (top row, Fig. 2D). When treated with MG132 for 2–4
185 hours, the chromatin-bound fraction of Orc6 was almost equivalent to the total fraction
186 (Supplementary information "Blot transparency"), indicating that most Orc6 binds to
187 chromatin upon inhibition of proteasome activity. The amount of Cdt1 was also
188 examined as a control to confirm the effect of the proteasome inhibitor. Cdt1 levels

189 increased over time in both whole-cell lysates (approximately 7-fold) and chromatin
190 fractions (approximately 3-fold) after MG132 treatment. Orc2 levels remained relatively
191 unchanged, with only a slight increase (1.2–1.5-fold). These results are consistent with
192 the single-plot analysis (Fig. 2A, B, S3D, E), suggesting that Orc6 dissociates from
193 chromatin during the S-phase via proteasome activity, without undergoing degradation.
194

195 **IMR90 cells with repeated passages exhibit high levels of chromatin-bound Orc6**
196 **after S-phase completion**

197 In our examination of Orc6 protein levels across various cell types, we observed that
198 IMR90 cells (human diploid fibroblasts) undergoing repeated passages displayed both
199 high levels of chromatin-bound Orc6 and enlarged nuclei (Fig. 3A). To explore the
200 relationship between cellular aging and pre-RC formation, we analyzed the dynamics of
201 chromatin-bound Orc6 and MCM levels during the cell cycle in IMR90 cells at different
202 passage numbers (Fig. 3A). Cells from passage 18 (younger cells) and passage 32 (older
203 cells, containing cells with large nuclei) were fixed using the pre-extraction method and
204 stained with Hoechst, anti-Orc6, and anti-Mcm2 antibodies. Single-cell plot analysis
205 showed that in passage 18 cells, the dynamics of chromatin-bound Orc6 and Mcm2
206 throughout the cell cycle were similar to those seen in hTERT-RPE1 cells (Fig. S4A).
207 Specifically, chromatin-bound Mcm2 levels increased during G1-phase, peaked at the
208 G1/S transition, and then decreased during the S-phase, reaching their lowest levels in
209 G2-phase (upper right panel in Fig. 3B) (Håland et al., 2015; Hayashi-Takanaka et al.,
210 2021; Zeng et al., 2023; Zhou et al., 2020). Chromatin-bound Orc6 levels were high in
211 G1-phase and decreased during S/G2-phase, similar to those seen in hTERT-RPE1 cells
212 (upper left panel in Fig.3B, second right in Fig. S2B). However, in passage 32 cells, a

213 subset of cells exhibited abnormally high levels of Orc6 (Orc6 >0.85 on the $\log_2$ scale)
214 after DNA replication was completed (1.8<Hoechst <2.1, magenta dots in the Orc6
215 panel, lower left panel in Fig. 3B). When these cells with high Orc6 levels (magenta
216 dots) were plotted on the Mcm2 panel, most of them displayed elevated Mcm2 levels
217 (red-boxed region, Fig. 3B) instead of the expected lower levels (blue-boxed region,
218 Fig. 3B). This suggests that in passage 32 IMR90 cells, pre-RC formation, which
219 normally occurs in G1 phase, was abnormally retained in G2 phase. These cells
220 progressed further through the cell cycle, resulting in the formation of cells with large
221 nuclei (2<Hoechst<4 in lower panels, Fig. 3B). Such cells were rarely observed in
222 passage 18 (upper left panel in Fig. 3B). In passage 18 (young cells), low levels of SA-
223 βGal and p21 protein, markers of cellular senescence, were observed (Fig. S4A). In
224 contrast, in passage 32 (aged cells, often containing large nuclei), some cells exhibited
225 high levels of SA-βGal and/or p21 protein (Fig. S4A). These results indicate that
226 IMR90 cells undergo cellular senescence between 18 and 32 passages. Given that
227 cellular senescence is known to be induced by impaired proteasome function
228 (Chondrogianni et al., 2003; Sabath et al., 2020), we hypothesized that the emergence of
229 cells with abnormal loading of Orc6 and MCM is related to the reduction of proteasome
230 activity.
231
232 **Low proteasome activity causes aberrant loading of chromatin-bound Orc6 after**
233 **the S-phase**
234 To test this hypothesis, we examined whether the reduction of proteasome activity in
235 immortalized cells (hTERT-RPE1 cells) leads to the emergence of cells with high Orc6
236 and MCM loading on chromatin after replication, similar to passage 32 IMR90 cells. To

237 determine the concentrations of MG132 that reproduce cellular senescence, hTERT-
238 RPE1 cells were treated with various concentrations of MG132 for longer periods (18
239 hours). Whereas most cells died at high concentrations used in Figure 2 (> 625 nM), cell
240 death was less frequent at a lower concentration of 312 nM MG132. Thus, we applied
241 MG132 at 312 nM or lower concentrations in the following experiments.

242 As a marker of cellular senescence, we first examined the levels of p21, a cell
243 cycle inhibitor that increases upon MG132 treatment with p53 stabilization (Kwon et
244 al., 2002; Zhu et al., 2007). Western blot analysis and immunostaining revealed elevated
245 p21 protein levels in MG132-treated cells compared to the DMSO control (Fig. 4A, Fig.
246 S4C), suggesting that proteasome inhibition by MG132 induces cell cycle arrest.
247 Similarly, cells positive for SA-βGal (senescence-associated β-galactosidase), a
248 hallmark of cellular senescence, were not detected on day 2 of treatment but appeared
249 on day 6 (Fig. S4D). Conversely, Ki67, a protein expressed in all phases of the cell
250 cycle except G0 phase (Scholzen and Gerdes, 2000), was widespread in MG132-treated
251 cells on day 1 but had disappeared in some cells on day 4 (Fig. S4E). Therefore,
252 treatment with low concentrations of MG132 for 18-24 h primarily led to cell cycle
253 arrest, while continuous treatment over several days induced cellular senescence.

254 Next, we examined the effect of low MG132 concentrations on Orc6
255 dynamics throughout the cell cycle. hTERT-RPE1 cells were treated with 78, 156, and
256 312 nM MG132 for 18 h. Cells were fixed using the pre-extraction method and stained
257 with anti-Orc6, anti-Mcm3, and anti-Cdt1 antibodies (Fig. 4C), followed by single-cell
258 plot analysis (Fig. 4C). We used anti-Mcm3 instead of anti-Mcm2 due to compatibility
259 with immunostaining; previous single-cell plot analysis confirmed that chromatin-
260 bound Mcm2 and Mcm3 exhibit similar cell cycle dynamics (Fig. S4F) (Hayashi-

261 Takanaka et al., 2021). MG132 treatment produced cells with high levels of chromatin-
262 bound Orc6 and high DNA content, marked as magenta dots in Orc6 panels (Orc6 >0.5
263 on the $\log_2$ scale, Hoechst >1.8, Fig. 4C). The number of these magenta cells increased
264 with increasing MG132 concentrations, whereas few were observed in the control
265 DMSO cells (Fig. 4C). These cells marked in Orc6 panels were also magenta-marked in
266 the Mcm3 and Ctd1 panels (middle and lower panels, Fig. 4C). Some of these cells
267 exhibited low Mcm3 signals (blue arrows in Fig. 4B; the blue-boxed region in Fig. 4C),
268 while others exhibited high Mcm3 levels (red arrows in lower panels in Fig. 4B; red-
269 boxed region in Fig. 4C), suggesting that these cells are in an abnormal G2-phase state.
270 Co-staining with Cdt1 revealed that most magenta-marked cells also had relatively high
271 levels of Cdt1 (Fig. 4C). Based on these observations, we hypothesized that the red-
272 boxed cells with high Mcm3 levels represent G1-phase cells, where pre-RC formation
273 had occurred, and the cells were ready to enter the S-phase.
274 To confirm the involvement of proteasomes in the abnormal pre-RC
275 formation after the S-phase, we examined the effects of depleting PSMD7, a subunit of
276 the 26S proteasome necessary for proteolytic activity (Shi et al., 2018), using siRNA
277 treatment. Cells were treated with PSMD7-targeting siRNA for 2 days, and Western
278 blotting showed that PSMD7 levels were reduced to approximately 20% of those in
279 control siRNA-treated cells (Fig. 4D). Under these conditions, cells were fixed using the
280 pre-extraction method, stained with anti-Orc6 and anti-Mcm2 antibodies, and subjected
281 to single-cell plot analysis (Fig. 4E, Fig. S4F). The results showed that PSMD7
282 depletion led to cells with high chromatin-bound Orc6 levels and high DNA content
283 (magenta dots, Orc6 >0.5 on the $\log_2$ scale, Hoechst >1.8, Fig. 4E). Some of these cells
284 had low Mcm2 levels (blue-boxed region, Fig. 4E), whereas others had high Mcm2

285 levels (red-boxed region, Fig. 4E), suggesting that proteasomal defects contribute to the
286 abnormal loading of Orc6 onto chromatin after the S-phase.
287 To investigate whether Orc6 binding to chromatin depends on Cdt1, we
288 examined the turnover of Cdt1. As the degradation of Cdt1 is regulated by enzymes
289 with NEDD8-activating enzyme activity (Lin et al., 2010), we suppressed Cdt1
290 degradation by treating cells with MLN4924, an inhibitor of the NEDD8-activating
291 enzyme. Treatment with 250 nM MLN4924 for 24 h significantly increased chromatin-
292 bound Cdt1 levels after the S phase; however, Orc6 levels did not increase beyond those
293 observed in the G1 phase, and MCM did not show abnormal loading (Fig. 4F). These
294 results suggest that the chromatin-bound Orc6 is regulated by the proteasome activity
295 and is not directly dependent on the presence of Cdt1 on chromatin.
296
297 **Inhibition of proteasome activity causes pre-RC formation without mitosis**
298 To examine whether cells with high levels of Orc6 and MCM, accompanied by high
299 DNA content (red box in Fig. 4C), appear without entering mitosis due to MG132
300 treatment, we performed a time-course analysis to determine the timing of their
301 appearance. We examined cell cycle progression using anti-Mcm2 antibody and anti-
302 histone H3 serine 10 phosphorylation (H3S10ph; an M-phase marker) antibodies
303 (Hayashi-Takanaka et al., 2009). In the case of control treated with DMSO, cells with
304 high histone H3S10ph signals were observed (Fig. 5A; magenta dots, bottom left in Fig.
305 5B), indicating normal cell cycle progression. The percentage of histone H3S10ph-
306 positive cells (magenta dots, ~5% of total) is consistent with the duration of mitosis in
307 hTERT-RPE1 cells from our previous study (~1 h, Hayashi-Takanaka et al., 2009;
308 Hayashi-Takanaka et al., 2021). In contrast, after MG132 treatment, cells with high

309 histone H3S10ph signals gradually disappeared by 8 h. During the first 4–12 h of
310 treatment, cells with high DNA content (Hoechst ~2) and low Mcm2 levels gradually
311 increased (blue-circled regions, Fig. 5B), suggesting accumulation of G2-phase cells.
312 Prolonged MG132 treatments (16–24 h) led to an increase in cells with high DNA
313 content (Hoechst ~2) and high Mcm2 levels (red-boxed regions, Fig. 5B), while no M-
314 phase cells were detected. These results suggest that cells with high DNA content
315 (Hoechst, ~2) and high Mcm2 levels represent tetraploid G1 cells produced by skipping
316 the M phase.
317 Using the same conditions, we analyzed the dynamics of chromatin-bound
318 Orc6 and Cdt1. Chromatin-bound Orc6 levels increased in S-phase cells by 4 h after
319 MG132 addition (upper panel in Fig. 5C), similar to those observed with higher
320 concentrations of MG132 (20 μM, Fig. 2). Chromatin-bound Cdt1 levels showed little
321 change 4 h after treatment (Fig. 5C) but increased by 8 h in cells with Hoechst value
322 around 2. The number of cells with high Orc6 and Cdt1 levels continued to increase by
323 12 h (orange-boxed regions, Fig. 5C), while cells with high levels of MCM appeared
324 later at 16-20 h (red-boxed regions, Fig. 5B). These results suggest that MCM does not
325 immediately bind to chromatin following the binding of Orc6 and Cdt1. We also
326 performed experiments combining MCM and Orc6 and obtained essentially the same
327 results (Fig. S5).
328
329 **Cells forming pre-RC via proteasome inhibition can progress through the cell cycle**
330 **as tetraploids**
331 In assessing cells with high DNA content and elevated levels of Orc6 and MCM on
332 chromatin, we hypothesized that these cells are in the tetraploid G1 phase and may

333 subsequently progress through the cell cycle. To test this hypothesis, cells were treated
334 with 312 nM MG132 for 24 h (day 1), washed, and then cultured in MG132-free
335 medium for an additional 24 h (day 2) (Fig. 6A). EdU was added to the culture medium
336 30 min before fixation at the end of both days to label cells undergoing DNA
337 replication. Cells were then fixed using the pre-extraction method and stained with anti-
338 Mcm2, and anti-Orc6 antibodies (Fig. 6B), and subjected to single-cell plot analysis
339 (Fig. 6C). EdU-positive cells were marked as orange dots, and the same cells were also
340 identified in the Mcm2 and Orc6 panels (Fig. 6C). On day 1, the number of EdU-
341 positive cells was limited, with most cells arrested at Hoechst levels of 1 or 2. Among
342 the cells with Hoechst levels around 2, a subset exhibited high levels of Mcm2 (red-
343 boxed regions: Hoechst >1.8 and Mcm2 >−1.5 on the $\log_2$ scale), accounting for 33.3
344 ±3.7% of the total (mean and standard error of the mean in three independent
345 experiments, Fig. 6B). On day 2, after MG132 removal, EdU-positive cells appeared in
346 the Hoechst range of 2–4 (orange arrows in Fig.6B; orange dots in day 2 panels),
347 comprising 7.68 ±0.40 % of the total (mean and standard error of the mean in three
348 independent experiments, Fig. 6B). These results indicate that cells with Hoechst levels
349 of 2–4 underwent another round of DNA replication, suggesting whole-genome
350 duplication (EdU panels, day 2, Fig. 6C). The Mcm2 patterns were similar between
351 cells with Hoechst levels 1–2 and 2–4 (Mcm2 panel, day 2, Fig. 6C), with Mcm2 levels
352 increasing in G1-phase and decreasing during S-phase, reaching their lowest levels in
353 G2-phase. These results suggest that the cells with high MCM levels after S-phase
354 induced by proteasome inhibition (red-boxed region, Fig. 6C) were in G1-phase of
355 tetraploidy, capable of undergoing an additional round of DNA replication.

356 To further clarify the cell cycle phases of cells with high Orc6 levels and a
357 Hoechst value around 2, these cells were marked as magenta dots in the Orc6 panels
358 (Orc6 > 0.5 on the $\log_2$ scale, Fig. 6C'). The same cells were also marked as magenta
359 dots in the Mcm2 panels (Fig. 6C'). As observed in Fig. 4D, the population of cells with
360 high Orc6 and Hoechst ~2 on day 1 split into two groups (Fig. 6C'): one with high
361 Mcm2 levels and the other with relatively low Mcm2 levels (red and blue arrows,
362 respectively, Fig.6B; red- and blue-boxed regions, respectively, Fig. 6C'). On day 2,
363 however, most of the high Orc6 population exhibited high Mcm2 levels. These results
364 suggest that Orc6 binds to chromatin before MCM loading, followed by the next
365 replication phase.
366
367 **Involvement of Orc6 in MCM loading in mitosis-skipped cells**
368 To determine whether the presence of Orc6 on chromatin after S-phase entry contributes
369 to MCM loading, we investigated MCM levels on chromatin following Orc6 depletion
370 via siRNA in hTERT-RPE1 cells (Fig. 7). First, we examined the effect of Orc6 siRNA
371 (siOrc6) on MCM loading during G1-phase, together with Orc1, which is a subunit
372 essential for MCM loading (Coulombe et al., 2019; Ogawa et al., 1999; Samson et al.,
373 2016) and is known to be degraded in a proteasome-dependent manner after the S-phase
374 entry (Li and DePamphilis, 2002; Méndez et al., 2002; Tatsumi et al., 2003). Western
375 blot analysis confirmed the efficient depletion of both Orc1 and Orc6 after 42 h of
376 siRNA treatment (Fig. 7A, B). Then, cells were fixed using the pre-extraction method,
377 stained with Hoechst and anti-Mcm2 antibody, and subjected to single-cell plot
378 analysis. Single-cell plot analysis showed that cells treated with siOrc1 or siOrc6
379 accumulated at G1 phase (81.0% and 71.3%, middle and right panels, respectively in

380 Fig. 7C) compared with control siRNA (66.2%, left panel in Fig. 7C). To quantify
381 MCM loading, cells with high MCM levels (cyan dots, half of the maximum value of
382 Mcm2 in Hoechst <1.125, Fig. 7C) were expressed as a percentage of the cells with
383 Hoechst signals >1.125 (Fig. 7D). The percentage of cells with high MCM levels was
384 significantly reduced in Orc1-depleted cells (3.8 ± 0.8% compared to 26.4 ± 6.8% in
385 siControl; Fig. 7D). Orc6 depletion caused a relatively small reduction in Mcm2 loading
386 (9.6 ± 2.3% in Fig. 7D). These results suggest that Orc6 plays a supporting role, while
387 Orc1 plays a critical role in MCM loading.

388 We next examined the effect of Orc6 depletion on Mcm2 loading induced by
389 proteasome inhibition. Cells were treated with siRNA for 18 h, followed by MG132
390 treatment for 24 h while maintaining siRNA treatment (Fig. 7E). After treatment, cells
391 were fixed using the pre-extraction method, stained with Hoechst and anti-Mcm2
392 antibody, and analyzed using single-cell plot analysis (Fig. 7F; Fig. S6A). Cells with
393 doubled DNA content (Hoechst ~2) accumulated by MG132 treatment in all siControl,
394 siOrc1 and siOrc6 (Fig. 7F). Cells with high MCM levels and Hoechst ~2 (magenta
395 dots, Hoechst >1.8 and Mcm2 >−1.5 on the $\log_2$ scale, Fig. 7F) were quantified as a
396 percentage of the total cells with Hoechst >1.8 (Fig. 7G). Orc1 depletion reduced the
397 percentage of high-MCM cells to 5.7 ± 1.2% (Fig. 7G), underscoring the importance of
398 Orc1 in MCM loading in tetraploid G1 cells. Orc6 depletion modestly reduced the
399 percentage of high-MCM cells (13.3 ± 4.2%) compared to the siControl (35.2 ± 3.4%).
400 These results suggest that while Orc6 contributes to MCM reloading in tetraploid G1
401 cells, its role is less prominent than that of Orc1.

402 We also examined a role of Cdc6, another pre-RC component, in MCM
403 loading after siRNA treatment. Western blot analysis confirmed effective Cdc6

404 reduction (Fig. 7H). Cells were treated with siCdc6 for 18 h, followed by MG132 for 24
405 h (Fig. 7E). The cells were then fixed using the pre-extraction method and stained with
406 Hoechst and anti-Mcm2 antibody. Single-cell plot analysis revealed a reduction in
407 tetraploid G1 cells high MCM levels (magenta dots, Hoechst >1.8, and Mcm2 >−1.5 on
408 the $\log_2$ scale) after Cdc6 depletion (Fig. 7I, J; Fig. S6B), similar to the effect of Orc6
409 depletion. This suggests that Orc6 contributes as much as Cdc6 to MCM loading during
410 the tetraploid G1-phase in hTERT-RPE1 cells.
411 In summary, during G1-phase, Orc6 binds to chromatin along with other pre-
412 RC components. Upon S-phase entry, Cdt1 and Orc1 are degraded by proteasome
413 activity, while Orc6 dissociates from chromatin (Fig. 8A). Orc2–5 remain bound to
414 chromatin throughout the cell cycle. These cells proceed through mitosis, producing
415 normal diploid cells (Fig. 8A). However, in cells with reduced proteasome activity,
416 Orc6, Orc1, Cdt1, and MCM are reloaded onto chromatin. These cells bypass mitosis
417 and proceed into replication, leading to tetraploid formation (Fig. 8B).
418
419 **Discussion**
420 In this study, we demonstrated dynamic changes in chromatin-bound Orc6 levels during
421 the cell cycle in hTERT-RPE1 cells. The levels of chromatin-bound Orc6 increased
422 until the G1/S transition, decreased upon entry into the S-phase, and remained low until
423 the next G1-phase, despite the total amount of Orc6 remaining almost unchanged
424 throughout the cell cycle. Contrary to our results, previous western blot analysis using
425 synchronized HeLa cells showed that chromatin-bound Orc6 levels remained nearly
426 constant across different cell cycle phases (Méndez et al., 2002). However, our single-
427 cell plot analysis revealed a more pronounced difference in Orc6 levels between G1 and

428 S/G2 phases in normal cell lines (IMR90, and hTERT-RPE1 cells) compared to cancer
429 cell lines (HeLa and U2OS cells) (Fig. 1, Fig. S2). This suggests that the regulation of
430 chromatin-bound Orc6 during the cell cycle could serve as a distinguishing factor
431 between normal and cancerous cells.

432 We further demonstrated that the removal of Orc6 from chromatin after the S-
433 phase, through a proteasome-dependent mechanism, plays a crucial role in preventing
434 abnormal MCM loading. Aberrant MCM loading beyond the S-phase can initiate an
435 additional round of DNA replication without mitotic division, leading to tetraploidy,
436 which may contribute to cancer development. To prevent such occurrences, the
437 ubiquitin-proteasome system regulates the levels of several pre-RC factors, such as
438 Cdt1, Cdc6, and Orc1, at specific cell cycle phases (Li and DePamphilis, 2002; Méndez
439 et al., 2002; Nishitani et al., 2006; Tatsumi et al., 2003; Walter et al., 2016).
440 Interestingly, unlike other pre-RC factors, Orc6 is not degraded at the protein level but
441 is instead dissociated from chromatin via proteasome activity. This indicates that the
442 proteasome regulates pre-RC protein levels on chromatin in a distinct manner, thereby
443 preventing abnormal MCM loading. Certain carcinomas exhibit elevated Orc6 levels
444 (Pan et al., 2022; Tang et al., 2023), suggesting that excess Orc6 might interfere with its
445 chromatin dissociation, potentially leading to the reloading of pre-RC onto chromatin.
446 Our results also suggest that eliminating Orc6 from chromatin at the onset of the S-
447 phase is critical. Given that Orc6 is the most evolutionarily diverse ORC subunit (Dhar
448 and Dutta, 2000), its dissociation from chromatin during the S-phase may represent an
449 auxiliary mechanism uniquely evolved to prevent aberrant MCM loading.

450 The precise molecular mechanism driving Orc6 dissociation from chromatin
451 remains unclear. Orc6 lacks known ubiquitinated amino acid residues for subsequent

452 proteasome degradation (Coulombe et al., 2019). One possibility is that the chromatin-
453 bound Orc6 levels are regulated by factors degraded through proteasome activity, such
454 as Orc1 or Cdt1. However, our experiments showed that reducing Orc1 and Cdt1 levels
455 did not affect the chromatin-bound Orc6 levels. Another plausible explanation involves
456 post-translational modifications, such as phosphorylation, as observed with *S. cerevisiae*
457 Orc6 (Chen and Bell, 2011; Chen et al., 2007). Notably, S-phase-specific
458 phosphorylation of Orc6 has been shown to contribute to genome stability via DNA
459 damage checkpoints (Lin et al., 2023). These modifications may facilitate Orc6
460 dissociation from chromatin, possibly mediated by the degradation of modifying
461 enzymes through proteasome activity. In addition, proteasomes may have non-
462 proteolytic functions. For example, the ATPase activity within the proteasome can
463 unwind DNA (Makino et al., 1996; Makino et al., 1999), suggesting that a proteasome
464 lacking proteolytic activity might still facilitate chromatin binding by ORC, including
465 Orc6. Furthermore, inhibition of proteasome activity has been associated with
466 nucleosome hyperacetylation at transcription start sites (Kinyamu et al., 2020), which
467 overlaps with replication origins (Sugimoto et al., 2018). This hyperacetylation may
468 promote Orc6 binding to chromatin.

469 A decline in proteasome activity affects a variety of cellular processes,
470 including senescence (Huang et al., 2022; Vilchez et al., 2014). Recent studies show
471 that cellular senescence is associated with a tetraploid state in G1-phase, which occurs
472 when cells bypass M-phase (Johmura et al., 2014; Panopoulos et al., 2014; Zeng et al.,
473 2023). In agreement, we observed that proteasome inhibition by MG132 led to
474 tetraploid G1 cells, and subsequent removal of the inhibitor restored proteasome
475 activity, promoting cell progression into S-phase (Figs. 4, 5). This implies that age-

476 related declines in proteasome activity may contribute to the production of tetraploid G1
477 cells, increasing the risk of cancer development.
478 In conclusion, our results show that normal cells can progress to a tetraploid
479 G1-phase when proteasome activity is reduced, a key step linked to whole-genome
480 duplication and carcinogenesis (Bielski et al., 2018; Gemble et al., 2022; López et al.,
481 2020). This study contributes to our understanding of the interplay between replication
482 factor dynamics and proteasome activity, further connecting these processes to
483 tetraploid cell formation, senescence, and cancer development.
484
485 **Materials and Methods**
486 **Antibodies for immunofluorescence staining and Western blotting**
487 The primary antibodies used were anti-Orc6 (1:300 for immunofluorescence staining
488 (IF) and 1:1000 for Western blot (WB); RRID:AB_670295, 3A4, sc-32735; Santa Cruz
489 Biotechnology), anti-Orc2 (1:300 for IF and 1:1000 for WB; RRID:AB_592395, M055-
490 3, MBL), anti-Cdt1 (1:300 for IF and 1:1000 for WB; RRID:AB_10896851, D10F11;
491 Cell Signaling Technology), anti-Mcm3 (1:1000 for IF; sc-390480; Lot#J1118, Santa
492 Cruz Biotechnology; 1:300 (IF); RRID:AB_398024, Anti-BM28; 610701, BD
493 transduction), anti-Mcm2 (1:1000 for IF and WB; RRID:AB_2142137, D7G11, Cell
494 Signaling Technology), anti-Orc1 (1:100 for IF and 1:300 for WB; F-10, sc-398734,
495 Santa Cruz Biotechnology), anti-GAPDH (1:1000 for WB; RRID:AB_1903993, 14C10;
496 Cell Signaling Technology), anti-histone H3 (1G1) (1:1000 for WB; Nozawa et al.,
497 2010), anti-PSMD7 (1:1000 for IF and WB; EPR13517, ab181072; Abcam), anti-Cdc6
498 (1:300 for IF and 1:1000 for WB,RRID:AB_627236, sc-9964, Santa Cruz
499 Biotechnology), anti-p21 (1:1000 for IF and WB; RRID:AB_823586, 12D1; Cell

500 Signaling Technology), and anti-histone H3S10ph (1:2000 for IF; CMA311, (Hayashi-
501 Takanaka et al., 2009)). The specificity of these antibodies used for immunostaining is
502 shown in Fig. S1. We previously confirmed by single-cell plot analysis based on
503 immunostaining that chromatin-bound Mcm2 and Mcm3 showed similar dynamics
504 during the cell cycle (Hayashi-Takanaka et al., 2021).
505 For fluorescent staining, the secondary antibodies were as follows: Alexa 488
506 donkey anti-mouse IgG (RRID:AB_2341099, 715-545-151; Jackson ImmunoResearch),
507 Cy5 donkey anti-mouse IgG (RRID:AB_2340820, 715-175-151; Jackson
508 ImmunoResearch), Cy3 donkey anti-Rat IgG (RRID:AB_2340667, 712-165-153;
509 Jackson ImmunoResearch), Alexa 488 donkey anti-rabbit IgG (RRID:AB_2313584,
510 711-545-152; Jackson ImmunoResearch) and Cy3 donkey anti-rabbit IgG
511 (RRID:AB_2340585, 711-005-152; Jackson ImmunoResearch).
512
513 **Cell culture and chemicals**
514 hTERT-RPE1 (ATCC, CRL-4000), IMR90 (ATCC, CCL-186), U2OS (ATCC, HTB-
515 96), and HeLa (RCB0007) cell lines were grown in a culture medium containing high-
516 glucose Dulbecco's modified Eagle's medium (Sigma-Aldrich) supplemented with
517 penicillin/streptomycin (100 units/mL penicillin, 100 μg/mL streptomycin; Fujifilm)
518 and 10% fetal calf serum (Thermo Fisher Scientific), as previously described. Unless
519 otherwise noted, the experiments were performed using hTERT-RPE1 cells.
520 siRNA transfection was performed using Lipofectamine RNAiMAX (Thermo
521 Fisher Scientific) with siRNAs (SASI_Hs01_00069342 for Orc6,
522 SASI_Hs01_00069343 for Orc6#2, SASI_Hs01_00038888 for Orc1,
523 SASI_Hs02_00341067 for Orc2, and Universal Negative Control #1, Sigma-Aldrich;

524 s11403 for PSMD7, s11401 for PSMD7#2, s2745 for Cdc6, and s2744 for Cdc6#2,
525 Ambion, Thermo Fisher Scientific) following the manufacturer's protocol.
526 MG132 (Fujifilm) and MLN4924 (MedChemExpress) were dissolved in
527 DMSO.
528
529 **Fluorescence staining for single-cell plot analysis**
530 Immunostaining was performed as previously described (Hayashi-Takanaka et al.,
531 2011; Hayashi-Takanaka et al., 2015; Hayashi-Takanaka et al., 2021). Briefly, the cells
532 (~2×10^4 cells/cm^2) were plated on a 12-well plate with a coverslip (15 mm diameter;
533 No. 1S; Matsunami) at the bottom and cultured for over 1 day.
534 In the direct fixation method, cells were first fixed with 1 mL of the fixative
535 (2% paraformaldehyde [Electron Microscopy Sciences] dissolved in 250 mM HEPES
536 [pH 7.4]) for 10 min at room temperature (approximately 25°C), followed by
537 permeabilization for 15 min using 1 % Triton X-100 in PBS, and subsequently blocked
538 with Blocking One (Nacalai Tesque, Inc.).
539 In the pre-extraction method, before fixation, cells were first treated with 1 mL
540 of 0.2% Triton X-100 solution containing 20 mM HEPES (pH 7.4), 100 mM NaCl, and
541 300 mM sucrose for 3 min on ice. After removing the Triton X-100 solution, the cells
542 were fixed using the fixative described above. This fixation method removes the nuclear
543 membranes and loosely bound chromatin proteins.
544 The fixed cells were incubated with specific primary antibodies (0.2–1 μg/mL)
545 for 2 h at room temperature (approximately 25°C) and washed three times (10 min
546 each) using PBS. When cells were stained with multiple antibodies, the cells were
547 simultaneously incubated with these antibodies. The cells were treated with secondary

548 antibodies (1 μg/mL) and Hoechst (0.1 μg/mL) for 2 h at room temperature
549 (approximately 25°C) and subsequently washed three times with PBS. The cells were
550 mounted using the ProLong Glass Antifade Mountant (Thermo Fisher Scientific).
551 The replication foci were labeled by culturing the cells in a medium containing
552 10 μM 5-ethynyl-2′-deoxyuridine (EdU) for 30 min. Subsequently, the cells were fixed
553 using the direct fixation or pre-extraction method, and the resulting EdU signals were
554 detected with Alexa Fluor 647 using a Click-iT EdU Imaging Kit (Thermo Fisher
555 Scientific).
556 For staining of SA-βGal (senescence-associated β-galactosidase), live cells
557 were treated with the reagents according to commercial protocols (Cellular Senescence
558 Detection Kit, SPiDER-βGal. Dojindo).
559
560 **Microscopy**
561 Fluorescence images were obtained using a DeltaVision Elite system (GE Healthcare
562 Inc.) equipped with a pco.edge 4.2 sCMOS camera (PCO) and an Olympus 40×
563 UApo/340 oil immersion objective lens (NA 0.65 with iris) with DeltaVision Elite Filter
564 Sets (DAPI-FITC-TRITC-Cy5).
565
566 **Single-cell plot analysis**
567 Single-cell plot analysis was used to measure the levels of multiple intracellular
568 components based on fluorescence microscopic images and plot their correlation in
569 individual cells (Hayashi-Takanaka et al., 2020; Hayashi-Takanaka et al., 2021). The
570 fluorescence intensity of each nucleus was measured using NIS Elements software
571 (version 3.0; Nikon). The background intensity outside the cells was subtracted. The

572 nuclear areas of individual cells were determined by automatic thresholding using
573 Hoechst signals. The sum of the intensities (i.e., the average intensity × nuclear area) in
574 each nucleus was measured across all the fluorescence channels. Cells in the M-phase
575 were excluded from analysis except those shown in Fig. 5B, 5C. In Fig. 5B, 5C, M-
576 phase cells were used for the analysis. To plot the Hoechst intensity distribution of 450–
577 600 nuclei, the signal intensity in each nucleus was normalized relative to those with the
578 20th lowest and 20th highest intensities, designated as 1 and 2, respectively, because
579 nuclei with the lowest and highest intensities were sometimes outliers. Hoechst intensity
580 was plotted on a linear scale. The average intensities of Orc6, EdU, Orc2, Cdt1, Mcm2,
581 and Mcm3 were set to 1 (0 on the $\log_2$ scale) and plotted on the $\log_2$ scale. The
582 fluorescence intensities were normalized to time "0 h" (Figs. 2A, 2B), DMSO treatment
583 (Figs. 4C, 4F), the negative control siRNA (Figs. 4E, 7C, 7F, 7I, S3A, S3C, S4G, S5C,
584 S5D) and MG132 treatment for day 1 (Fig. 6C). The values relative to the average were
585 plotted using Mathematica (version 13.0) (Wolfram Research).
586
587 **Preparation of chromatin fractions and whole-cell lysates**
588 Native chromatin fractions (hereafter, referred to as "chromatin fractions") were
589 prepared by the method previously described (Quan et al., 2015; Sheu and Stillman,
590 2006) with some modifications (Hayashi-Takanaka et al., 2021). The cells were washed
591 with cold PBS, suspended in buffer A (50 mM HEPES [pH 7.4], 100 mM KCl, 2.5 mM
592 $MgCl_2$, 0.1 mM $ZnSO_4$, 1 mM ATP, 1 mM dithiothreitol [DTT], and protease inhibitor
593 cocktail [EDTA-free, Nacalai Tesque, Inc.]), and collected via centrifugation (1,300 *g*, 3
594 min, 4°C). The cells were subsequently treated with 200 µL of 0.2% Triton X-100 in
595 buffer A, layered with 200 µL of 30% sucrose cushion in buffer A containing 0.2%

596 Triton X-100, and centrifuged at 20,000 × *g* for 10 min at 4°C. The pellets were
597 collected as chromatin fractions and dissolved in 1× SDS loading buffer. The
598 suspension was then subjected to SDS-PAGE.
599 To prepare whole-cell lysates, the cells were washed with PBS and suspended
600 in an equal volume of 2× SDS loading buffer. The suspension was subjected to SDS-
601 PAGE.
602
603 **Western blot analysis**
604 Chromatin fractions and whole-cell lysates were suspended in 1× SDS loading buffer
605 and subjected to 10%, 12%, or 15% SDS-PAGE to separate proteins. Proteins were
606 transferred onto Immobilon-P PVDF membranes (Merck) using a semi-dry blotting
607 system (ATTO). After blocking with 5% skim milk (Nacalai Tesque, Inc.), the
608 membranes were incubated with the primary antibodies. After incubation with
609 peroxidase-conjugated secondary antibodies (GE Healthcare), the signals were detected
610 using ImmunoStar LD (Fujifilm Wako) and the ChemiDoc image system (BioRad). The
611 intensity of the signals was quantified using Image Lab software (BioRad).
612
613 **Acknowledgements**
614 We thank Ms. Chizuru Ohtsuki and Yoshino Kubota for their technical assistance, and
615 Drs. Hisao Masai, Haruhiko Asakawa, and Yasuhiro Hirano for insightful discussion.
616 We also thank Dr. Hiroshi Kimura for histone H3 antibodies and Dr. Hisao Masukata for
617 critically reading the manuscript.
618 This work was supported by JSPS KAKENHI grants: JP18H05530,
619 JP20K20582 and JP20K08698 (to IH); JP18H05533, JP20H00454 and JP23K05636 (to

YH); and JP18H05528 (to TH). This work was also supported by the Naito Foundation, Urakami Foundation for Food and Food Culture Promotion, and the Foundation for Promotion of Cancer Research in Japan (to YHT).

Data Availability

Source data are available from the corresponding authors upon reasonable request.

Conflict of interest

The authors declare no competing interests.

630 **References**

631 **Balasov, M., Huijbregts, R. P. H. and Chesnokov, I.** (2009). Functional analysis of an
632 Orc6 mutant in Drosophila. *Proc Natl Acad Sci U S A* **106**, 10672–10677.

633 **Bell, S. D. and Botchan, M. R.** (2013). The minichromosome maintenance replicative
634 helicase. *Cold Spring Harb Perspect Biol* **5**, a012807.

635 **Bell, S. P. and Labib, K.** (2016). Chromosome Duplication in Saccharomyces cerevisiae.
636 *Genetics* **203**, 1027–1067.

637 **Bernal, J. A. and Venkitaraman, A. R.** (2011). A vertebrate N-end rule degron reveals
638 that Orc6 is required in mitosis for daughter cell abscission. *J Cell Biol* **192**, 969–
639 978.

640 **Bielski, C. M., Zehir, A., Penson, A. V., Donoghue, M. T. A., Chatila, W., Armenia, J.,**
641 **Chang, M. T., Schram, A. M., Jonsson, P., Bandlamudi, C., et al.** (2018).
642 Genome doubling shapes the evolution and prognosis of advanced cancers. *Nat*
643 *Genet* **50**, 1189–1195.

644 **Chen, S. and Bell, S. P.** (2011). CDK prevents Mcm2–7 helicase loading by inhibiting
645 Cdt1 interaction with Orc6. *Genes Dev.* **25**, 363–372.

646 **Chen, S., De Vries, M. A. and Bell, S. P.** (2007). Orc6 is required for dynamic recruitment
647 of Cdt1 during repeated Mcm2–7 loading. *Genes Dev.* **21**, 2897–2907.

648 **Chesnokov, I. N., Chesnokova, O. N. and Botchan, M.** (2003). A cytokinetic function of
649 *Drosophila* ORC6 protein resides in a domain distinct from its replication activity.
650 *Proc. Natl. Acad. Sci. U.S.A.* **100**, 9150–9155.

651 **Chondrogianni, N. and Gonos, E. S.** (2004). Proteasome inhibition induces a senescence-
652 like phenotype in primary human fibroblasts cultures. *Biogerontology* **5**, 55–61.

653 **Chondrogianni, N., Stratford, F. L. L., Trougakos, I. P., Friguet, B., Rivett, A. J. and**
654 **Gonos, E. S.** (2003). Central role of the proteasome in senescence and survival of
655 human fibroblasts: induction of a senescence-like phenotype upon its inhibition
656 and resistance to stress upon its activation. *J Biol Chem* **278**, 28026–28037.

657 **Coulombe, P., Nassar, J., Peiffer, I., Stanojcic, S., Sterkers, Y., Delamarre, A., Bocquet,**
658 **S. and Méchali, M.** (2019). The ORC ubiquitin ligase OBI1 promotes DNA

659 replication origin firing. *Nat Commun* **10**, 2426.

660 **Deegan, T. D. and Diffley, J. F.** (2016). MCM: one ring to rule them all. *Current Opinion*
661 *in Structural Biology* **37**, 145–151.

662 **Dhar, S. K. and Dutta, A.** (2000). Identification and Characterization of the Human
663 ORC6 Homolog. *Journal of Biological Chemistry* **275**, 34983–34988.

664 **Duncker, B. P., Chesnokov, I. N. and McConkey, B. J.** (2009). The origin recognition
665 complex protein family. *Genome Biol* **10**, 214.

666 **Feng, X., Noguchi, Y., Barbon, M., Stillman, B., Speck, C. and Li, H.** (2021). The
667 structure of ORC-Cdc6 on an origin DNA reveals the mechanism of ORC
668 activation by the replication initiator Cdc6. *Nat Commun* **12**, 3883.

669 **Ganier, O., Prorok, P., Akerman, I. and Méchali, M.** (2019). Metazoan DNA replication
670 origins. *Curr Opin Cell Biol* **58**, 134–141.

671 **Gemble, S., Wardenaar, R., Keuper, K., Srivastava, N., Nano, M., Macé, A.-S., Tijhuis,**
672 **A. E., Bernhard, S. V., Spierings, D. C. J., Simon, A., et al.** (2022). Genetic
673 instability from a single S phase after whole-genome duplication. *Nature* **604**,
674 146–151.

675 **Håland, T. W., Boye, E., Stokke, T., Grallert, B. and Syljuåsen, R. G.** (2015).
676 Simultaneous measurement of passage through the restriction point and MCM
677 loading in single cells. *Nucleic Acids Res* **43**, e150–e150.

678 **Hayashi-Takanaka, Y., Yamagata, K., Nozaki, N. and Kimura, H.** (2009). Visualizing
679 histone modifications in living cells: spatiotemporal dynamics of H3
680 phosphorylation during interphase. *J Cell Biol* **187**, 781–790.

681 **Hayashi-Takanaka, Y., Yamagata, K., Wakayama, T., Stasevich, T. J., Kainuma, T.,**
682 **Tsurimoto, T., Tachibana, M., Shinkai, Y., Kurumizaka, H., Nozaki, N., et al.**
683 (2011). Tracking epigenetic histone modifications in single cells using Fab-based
684 live endogenous modification labeling. *Nucleic Acids Research* **39**, 6475–6488.

685 **Hayashi-Takanaka, Y., Maehara, K., Harada, A., Umehara, T., Yokoyama, S., Obuse,**
686 **C., Ohkawa, Y., Nozaki, N. and Kimura, H.** (2015). Distribution of histone H4
687 modifications as revealed by a panel of specific monoclonal antibodies.
688 *Chromosome Res* **23**, 753–766.

689 **Hayashi-Takanaka, Y., Kina, Y., Nakamura, F., Becking, L. E., Nakao, Y., Nagase, T.,**
690 **Nozaki, N. and Kimura, H.** (2020). Histone modification dynamics as revealed
691 by multicolor immunofluorescence-based single-cell analysis. *J Cell Sci* **133**,
692 jcs243444.

693 **Hayashi-Takanaka, Y., Hayashi, Y., Hirano, Y., Miyawaki-Kuwakado, A., Ohkawa, Y.,**
694 **Obuse, C., Kimura, H., Haraguchi, T. and Hiraoka, Y.** (2021). Chromatin
695 loading of MCM hexamers is associated with di-/tri-methylation of histone
696 H4K20 toward S phase entry. *Nucleic Acids Res* **49**, 12152–12166.

697 **Hu, Y. and Stillman, B.** (2023). Origins of DNA replication in eukaryotes. *Mol Cell* **83**,
698 352–372.

699 **Huang, W., Hickson, L. J., Eirin, A., Kirkland, J. L. and Lerman, L. O.** (2022). Cellular
700 senescence: the good, the bad and the unknown. *Nat Rev Nephrol* **18**, 611–627.

701 **Ishimi, Y.** (2018). Regulation of MCM2-7 function. *Genes Genet Syst* **93**, 125–133.

702 **Johmura, Y., Shimada, M., Misaki, T., Naiki-Ito, A., Miyoshi, H., Motoyama, N.,**
703 **Ohtani, N., Hara, E., Nakamura, M., Morita, A., et al.** (2014). Necessary and
704 Sufficient Role for a Mitosis Skip in Senescence Induction. *Molecular Cell* **55**, 73–
705 84.

706 **Kinyamu, H. K., Bennett, B. D., Bushel, P. R. and Archer, T. K.** (2020). Proteasome
707 inhibition creates a chromatin landscape favorable to RNA Pol II processivity. *J*
708 *Biol Chem* **295**, 1271–1287.

709 **Kwon, Y. H., Jovanovic, A., Serfas, M. S., Kiyokawa, H. and Tyner, A. L.** (2002). P21
710 functions to maintain quiescence of p27-deficient hepatocytes. *J Biol Chem* **277**,
711 41417–41422.

712 **Li, C.-J. and DePamphilis, M. L.** (2002). Mammalian Orc1 Protein Is Selectively
713 Released from Chromatin and Ubiquitinated during the S-to-M Transition in the
714 Cell Division Cycle. *Molecular and Cellular Biology* **22**, 105–116.

715 **Limas, J. C. and Cook, J. G.** (2019). Preparation for DNA replication: the key to a
716 successful S phase. *FEBS Lett* **593**, 2853–2867.

717 **Lin, J. J., Milhollen, M. A., Smith, P. G., Narayanan, U. and Dutta, A.** (2010). NEDD8-
718 targeting drug MLN4924 elicits DNA rereplication by stabilizing Cdt1 in S phase,

719 triggering checkpoint activation, apoptosis, and senescence in cancer cells.
720 *Cancer Res* **70**, 10310–10320.

721 **Lin, Y.-C., Liu, D., Chakraborty, A., Kadyrova, L. Y., Song, Y. J., Hao, Q., Mitra, J.,**
722 **Hsu, R. Y. C., Arif, M. K., Adusumilli, S., et al.** (2022). Orc6 is a component of
723 the replication fork and enables efficient mismatch repair. *Proc Natl Acad Sci U*
724 *S A* **119**, e2121406119.

725 **Lin, Y.-C., Liu, D., Chakraborty, A., Macias, V., Brister, E., Sonalkar, J., Shen, L.,**
726 **Mitra, J., Ha, T., Kajdacsy-Balla, A., et al.** (2023). DNA Damage-Induced, S-
727 Phase Specific Phosphorylation of Orc6 is Critical for the Maintenance of Genome
728 Stability. *Mol Cell Biol* **43**, 143–156.

729 **Liu, S., Balasov, M., Wang, H., Wu, L., Chesnokov, I. N. and Liu, Y.** (2011). Structural
730 analysis of human Orc6 protein reveals a homology with transcription factor
731 TFIIB. *Proc. Natl. Acad. Sci. U.S.A.* **108**, 7373–7378.

732 **López, S., Lim, E. L., Horswell, S., Haase, K., Huebner, A., Dietzen, M., Mourikis, T.**
733 **P., Watkins, T. B. K., Rowan, A., Dewhurst, S. M., et al.** (2020). Interplay
734 between whole-genome doubling and the accumulation of deleterious alterations
735 in cancer evolution. *Nat Genet* **52**, 283–293.

736 **Makino, Y., Yogosawa, S., Kanemaki, M., Yoshida, T., Yamano, K., Kishimoto, T.,**
737 **Moncollin, V., Egly, J. M., Muramatsu, M. and Tamura, T.** (1996). Structures of
738 the rat proteasomal ATPases: determination of highly conserved structural
739 motifs and rules for their spacing. *Biochem Biophys Res Commun* **220**, 1049–
740 1054.

741 **Makino, Y., Yoshida, T., Yogosawa, S., Tanaka, K., Muramatsu, M. and Tamura, T. A.**
742 (1999). Multiple mammalian proteasomal ATPases, but not proteasome itself, are
743 associated with TATA-binding protein and a novel transcriptional activator,
744 TIP120. *Genes Cells* **4**, 529–539.

745 **Méndez, J., Zou-Yang, X. H., Kim, S.-Y., Hidaka, M., Tansey, W. P. and Stillman, B.**
746 (2002). Human Origin Recognition Complex Large Subunit Is Degraded by
747 Ubiquitin-Mediated Proteolysis after Initiation of DNA Replication. *Molecular*
748 *Cell* **9**, 481–491.

749 **Nishitani, H., Sugimoto, N., Roukos, V., Nakanishi, Y., Saijo, M., Obuse, C., Tsurimoto,**

750 **T., Nakayama, K. I., Nakayama, K., Fujita, M., et al.** (2006). Two E3 ubiquitin
751 ligases, SCF-Skp2 and DDB1-Cul4, target human Cdt1 for proteolysis. *EMBO J*
752 **25**, 1126–1136.

753 **Nozawa, R.-S., Nagao, K., Masuda, H.-T., Iwasaki, O., Hirota, T., Nozaki, N., Kimura,**
754 **H. and Obuse, C.** (2010). Human POGZ modulates dissociation of HP1alpha from
755 mitotic chromosome arms through Aurora B activation. *Nat Cell Biol* **12**, 719–
756 727.

757 **Ogawa, Y., Takahashi, T. and Masukata, H.** (1999). Association of fission yeast Orp1
758 and Mcm6 proteins with chromosomal replication origins. *Mol Cell Biol* **19**, 7228–
759 7236.

760 **Pan, Q., Li, F., Ding, Y., Huang, H. and Guo, J.** (2022). ORC6 acts as a biomarker and
761 reflects poor outcome in clear cell renal cell carcinoma. *J Cancer* **13**, 2504–2514.

762 **Panopoulos, A., Pacios-Bras, C., Choi, J., Yenjerla, M., Sussman, M. A., Fotedar, R.**
763 **and Margolis, R. L.** (2014). Failure of cell cleavage induces senescence in
764 tetraploid primary cells. *Mol Biol Cell* **25**, 3105–3118.

765 **Prasanth, S. G., Prasanth, K. V. and Stillman, B.** (2002). Orc6 Involved in DNA
766 Replication, Chromosome Segregation, and Cytokinesis. *Science* **297**, 1026–1031.

767 **Quan, Y., Xia, Y., Liu, L., Cui, J., Li, Z., Cao, Q., Chen, X. S., Campbell, J. L. and Lou,**
768 **H.** (2015). Cell-Cycle-Regulated Interaction between Mcm10 and Double
769 Hexameric Mcm2-7 Is Required for Helicase Splitting and Activation during S
770 Phase. *Cell Reports* **13**, 2576–2586.

771 **Sabath, N., Levy-Adam, F., Younis, A., Rozales, K., Meller, A., Hadar, S., Soueid-**
772 **Baumgarten, S. and Shalgi, R.** (2020). Cellular proteostasis decline in human
773 senescence. *Proc Natl Acad Sci U S A* **117**, 31902–31913.

774 **Samson, R. Y., Abeyrathne, P. D. and Bell, S. D.** (2016). Mechanism of Archaeal MCM
775 Helicase Recruitment to DNA Replication Origins. *Mol Cell* **61**, 287–296.

776 **Scholzen, T. and Gerdes, J.** (2000). The Ki-67 protein: from the known and the unknown.
777 *J Cell Physiol* **182**, 311–322.

778 **Semple, J. W., Da-Silva, L. F., Jervis, E. J., Ah-Kee, J., Al-Attar, H., Kummer, L.,**
779 **Heikkila, J. J., Pasero, P. and Duncker, B. P.** (2006). An essential role for Orc6

780 in DNA replication through maintenance of pre-replicative complexes. *EMBO J*
781 **25**, 5150–5158.

782 **Sheu, Y.-J. and Stillman, B.** (2006). Cdc7-Dbf4 Phosphorylates MCM Proteins via a
783 Docking Site-Mediated Mechanism to Promote S Phase Progression. *Molecular*
784 *Cell* **24**, 101–113.

785 **Shi, K., Zhang, J.-Z., Zhao, R.-L., Yang, L. and Guo, D.** (2018). PSMD7 downregulation
786 induces apoptosis and suppresses tumorigenesis of esophageal squamous cell
787 carcinoma via the mTOR/p70S6K pathway. *FEBS Open Bio* **8**, 533–543.

788 **Sugimoto, N., Maehara, K., Yoshida, K., Ohkawa, Y. and Fujita, M.** (2018). Genome-
789 wide analysis of the spatiotemporal regulation of firing and dormant replication
790 origins in human cells. *Nucleic Acids Res* **46**, 6683–6696.

791 **Tang, M., Chen, J., Zeng, T., Ye, D.-M., Li, Y.-K., Zou, J. and Zhang, Y.-P.** (2023).
792 Systemic analysis of the DNA replication regulator origin recognition complex in
793 lung adenocarcinomas identifies prognostic and expression significance. *Cancer*
794 *Med* **12**, 5035–5054.

795 **Tatsumi, Y., Ohta, S., Kimura, H., Tsurimoto, T. and Obuse, C.** (2003). The ORC1 Cycle
796 in Human Cells. *Journal of Biological Chemistry* **278**, 41528–41534.

797 **Thakur, B. L., Ray, A., Redon, C. E. and Aladjem, M. I.** (2022). Preventing excess
798 replication origin activation to ensure genome stability. *Trends Genet* **38**, 169–
799 181.

800 **Torres, C., Lewis, L. and Cristofalo, V. J.** (2006). Proteasome inhibitors shorten
801 replicative life span and induce a senescent-like phenotype of human fibroblasts.
802 *J Cell Physiol* **207**, 845–853.

803 **Ukekawa, R., Maegawa, N., Mizutani, E., Fujii, M. and Ayusawa, D.** (2004).
804 Proteasome inhibitors induce changes in chromatin structure characteristic of
805 senescent human fibroblasts. *Biosci Biotechnol Biochem* **68**, 2395–2397.

806 **Vassilev, A. and DePamphilis, M.** (2017). Links between DNA Replication, Stem Cells
807 and Cancer. *Genes* **8**, 45.

808 **Vilchez, D., Saez, I. and Dillin, A.** (2014). The role of protein clearance mechanisms in
809 organismal ageing and age-related diseases. *Nat Commun* **5**, 5659.

Walter, D., Hoffmann, S., Komseli, E.-S., Rappsilber, J., Gorgoulis, V. and Sørensen, C. S. (2016). SCFCyclin F-dependent degradation of CDC6 suppresses DNA re-replication. *Nat Commun* **7**, 10530.

Xu, N., You, Y., Liu, C., Balasov, M., Lun, L. T., Geng, Y., Fung, C. P., Miao, H., Tian, H., Choy, T. T., et al. (2020). Structural basis of DNA replication origin recognition by human Orc6 protein binding with DNA. *Nucleic Acids Research* **48**, 11146–11161.

Zeng, J., Hills, S. A., Ozono, E. and Diffley, J. F. X. (2023). Cyclin E-induced replicative stress drives p53-dependent whole-genome duplication. *Cell* **186**, 528-542.e14.

Zhou, Y., Pozo, P. N., Oh, S., Stone, H. M. and Cook, J. G. (2020). Distinct and sequential re-replication barriers ensure precise genome duplication. *PLoS Genet* **16**, e1008988.

Zhu, Q., Wani, G., Yao, J., Patnaik, S., Wang, Q.-E., El-Mahdy, M. A., Praetorius-Ibba, M. and Wani, A. A. (2007). The ubiquitin-proteasome system regulates p53-mediated transcription at p21waf1 promoter. *Oncogene* **26**, 4199–4208.

826 **Figure Legends**

827

828 **Figure 1. Detection of chromatin-bound Orc6 by single-cell plot analysis**

829 (**A**) Representative fluorescence images of Hoechst, EdU, Orc6, Orc2, and merged
830 (Hoechst/EdU/Orc6) in hTERT-RPE1 cells prepared using the direct fixation method
831 (upper panels) and the pre-extraction method (lower panels). Scale bars, 10 µm. (**B**)
832 Single-cell plot analysis based on the images in (**A**). Each dot represents the EdU, Orc6,
833 and Orc2 intensities in a single individual cell against the Hoechst intensities. The
834 orange dots represent S-phase cells based on EdU intensities ($\log_2$[EdU] > −2). n = 450
835 (number of cells examined in each panel).

836

837 **Figure 2. Effects of proteasome inhibitors on the dynamics of Orc6 during the cell**
838 **cycle**

839 Single-cell plot analysis of Orc6 (top), Cdt1 (middle), and Orc2 (bottom) in hTERT-
840 RPE1 cells. Cells were treated with 20 µM MG132 for 0, 1, 2, or 4 h (timescale on the
841 top), fixed using the direct fixation method (left panels) and the pre-extraction method
842 (right panels). Each dot represents the intensity of Orc6, Cdt1, and Orc2 in a single
843 individual cell plotted against the Hoechst intensity. n = 450 (number of cells examined
844 in each panel). (**B**) Orc6, Cdt1, and Orc2 levels in the S-phase cells. Cells
845 corresponding to the S-phase (1.1 < Hoechst < 1.75) were selected from (**A**), and their
846 fluorescence intensities were plotted. The average intensity in MG132-untreated cells (0
847 h) was defined as 1. G1- and G2-phase cells are shown in Fig. S3D, E. (**C**) Schematic
848 diagram of the biochemical fractionation method for whole-cell lysates and chromatin
849 fractions. (**D**) Western blot analysis using antibodies against Orc6, Cdt1, Orc2, histone
850 H3, and GAPDH. hTERT-RPE1 cells were treated with 20 µM MG132 for the indicated
851 periods (h). Whole-cell lysates (left) and chromatin fractions (right) were prepared and
852 analyzed using western blotting. Histone H3 and GAPDH are loading controls.
853 Molecular weight markers (kDa) are indicated on the right.

854

855 **Figure 3. Aberrantly high levels of chromatin-bound Orc6 and Mcm2 in aged**
856 **fibroblast cells**

857 (**A**) IMR90 cells (passage numbers 18 and 32) were fixed using the pre-extraction
858 method and stained using Hoechst, anti-Orc6, and anti-Mcm2 antibodies.
859 Representative fluorescence images are shown. Arrows indicate relatively larger nuclei
860 with high Orc6 signals. Scale bars, 10 µm. (**B**) Single-cell plot analysis based on the

861 images in (**A**). Each dot represents the intensity of Orc6 and Mcm2 in an individual cell
862 plotted against Hoechst intensity. In the range of 1.8 < Hoechst < 2.1, the magenta dots
863 in the Orc6 panels represent cells with fluorescent signals of $\log_2$(Orc6) > 0.85. The
864 same cells are also marked magenta in the Mcm2 panels. The red-boxed regions
865 represent cells with high MCM levels ($\log_2$[Mcm2] > −1.5), and the blue-boxed regions
866 represent cells with low MCM levels ($\log_2$[Mcm2] < −1.5) in the range of 1.8 < Hoechst
867 < 2.1. n = 450 (number of cells examined in each panel).
868
869 **Figure 4. MG132 treatment increases the cells with high chromatin-bound Orc6**
870 **after the S-phase**
871 (**A**) Western blot analysis of whole-cell lysates using antibodies against p21 (cell cycle
872 marker) and GAPDH (loading control). hTERT-RPE1 cells were treated with DMSO or
873 312 nM MG132 for 1 day before harvesting. Molecular weight markers (kDa) are
874 indicated on the right. (**B**) Representative fluorescence images of Hoechst, Orc6, Mcm3,
875 and Cdt1 staining in hTERT-RPE1 cells treated with DMSO or 312 nM MG132 for 18
876 h. Cells were fixed using the pre-fixation method and stained with Hoechst, anti-Orc6,
877 anti-Mcm3, and anti-Cdt1 antibodies. G1 (yellow arrows) and G2 (blue arrows) were
878 labeled based on single-cell plot analysis in (**C**). Red arrows indicate a representative
879 cell categorized in the red-boxed region in (**C**). Scale bars, 10 μm. (**C**) Single-cell plot
880 analysis based on images of hTERT-RPE1 cells treated with DMSO or the indicated
881 concentration of MG132, fixed and stained as described in (B). The cells with high Orc6
882 levels ($\log_2$[Orc6] > 0.5) and high DNA content (Hoechst > 1.8) are marked magenta in
883 the Orc6 panels. The same cells are also marked magenta in the Mcm3 and Cdt1 panels.
884 The red-boxed region represents cells with high Mcm3 levels and high DNA content,
885 and the blue-boxed region represents cells with low Mcm3 levels and high DNA
886 content. n = 450 (cells examined in each panel). (**D**) Efficiency of siRNA knockdown of
887 PSMD7. Western blot analysis of hTERT-RPE1 cell lysates was performed with
888 antibodies against PSMD7 and GAPDH (loading control) after 2 days of siRNA
889 treatment. Molecular weight markers (kDa) are indicated on the right. (**E**) Single-cell
890 plot analysis of Orc6 and Mcm2 in hTERT-RPE1 cells treated with siControl or
891 siPSMD7. Cells were treated with siRNA for 2 days, fixed, and stained with Hoechst,
892 anti-Orc6, and anti-Mcm2 antibodies. Cells with high Orc6 levels ($\log_2$[Orc6] > 0.5)
893 and high DNA content (Hoechst > 1.8) are marked magenta in the Orc6 panels. The
894 same cells are also marked magenta in the Mcm2 panels. The red-boxed region
895 represents cells with high Mcm2 levels ($\log_2$[Mcm2] > −1.5) and high DNA content
896 (Hoechst > 1.8), and the blue-boxed region represents cells with low Mcm2 levels

897 ($\log_2$[Mcm2] < −1.5) and high DNA content (Hoechst > 1.8). n = 500 (number of cells
898 examined in each panel). Another experiment with a different siRNA is shown in Fig.
899 S6A. (**F**) Single-cell plot analysis of hTERT-RPE1 cells treated with DMSO or 250 nM
900 MLN4924 for 24 h. The cells were fixed using the pre-extraction method, and stained
901 with Hoechst, anti-Orc6, anti-Mcm3, and anti-Cdt1 antibodies. n = 450 (number of cells
902 examined in each panel).
903
904 **Figure 5. Time course of MG132-induced changes in Orc6, Mcm2 and Cdt1**
905 **indicate abnormal Pre-RC formation without mitosis**
906 (**A**) Images of Hoechst, Mcm2, histone H3S10ph, and EdU in the DMSO-treated cells
907 fixed using the pre-extraction method. Combination of Mcm2, EdU and histone
908 H3S10ph signals identify cells in G1, S, G2, and M phases. The merged image shows
909 Hoechst (blue), Mcm2 (red), and histone H3S10ph (green). Scale bar, 10 µm. (**B**)
910 Single-cell plot analysis of Mcm2 (top), histone H3S10ph (bottom) in cells treated with
911 DMSO or 312 nM MG132 for the indicated durations. Cells with high H3S10ph levels
912 ($\log_2$[H3S10ph] > 1) are marked magenta in the H3S10ph panels. Blue-circled regions
913 represent cells with low Mcm2 levels and high DNA content. Red-boxed regions
914 represent cells with high Mcm2 and high DNA content. n = 425 (number of cells
915 examined in each panel). (**C**) Single-cell plot analysis of Orc6 (top) and Cdt1 (bottom)
916 in hTERT-RPE1 cells treated with DMSO or 312 nM MG132 for the indicated
917 durations. Orange-boxed regions represent cells with high Orc6, Cdt1, and high DNA
918 content in the 12-h treatment.
919
920 **Figure 6. Cells forming pre-RC via proteasome inhibition can progress through the**
921 **cell cycle as tetraploids**
922 (**A**) Timing diagram for MG132 treatment and EdU labeling used in (**B)** and **(C**).
923 hTERT-RPE1 cells were incubated with 312 nM MG132 for a day (day 1) (left panels in
924 **B**), washed with fresh medium without MG132, and incubated for another day (day 2)
925 (right panels in **B**). The cells were labeled with EdU for 30 min before the sample
926 collection on day 1 and day 2. (**B**) Representative fluorescence images of Hoechst,
927 Orc6, and Mcm2 staining used in single-cell plot analysis in (**C** and **C'**). Red and blue
928 arrows indicate typical cells in the red and blue boxes in (**C** and **C'**). Orange arrows
929 indicate a tetraploid S-phase cell (orange dots of day 2 in **(C)).** Scale bars, 10 µm. (**C**)
930 Single-cell plot analysis of EdU (top), Mcm2 (middle), and Orc6 (bottom). The orange
931 dots represent S-phase cells based on EdU intensities ($\log_2$[EdU] > 2) with high DNA
932 contents (Hoechst > 1.8). The red-boxed regions represent cells with high Mcm2 levels

933 ($\log_2$[Mcm2] > −1.5) and high DNA contents (1.8 < Hoechst < 2.1). n = 600 (cells
934 examined in each panel). (**C'**) The same data from (**C**) is reused but marked differently.
935 Cells with high Orc6 levels ($\log_2$[Orc6] > 0.5) and high DNA content (Hoechst > 1.8)
936 are marked magenta in the Orc6 panels. The same cells are also marked magenta in the
937 Mcm2 panels. The red-boxed region represents cells with high Mcm2 levels
938 ($\log_2$[Mcm2] > −1.5) and high DNA content (1.8 < Hoechst < 2.1). The blue-boxed
939 region represents cells with low Mcm2 levels ($\log_2$[Mcm2] < -1.5) and high DNA
940 content (1.8 < Hoechst < 2.1).
941
942 **Figure 7. Effects of Orc6 depletion on the formation of tetraploid cells**
943 (**A**) Schematic diagram of siRNA treatment timing. hTERT-RPE1 cells were treated
944 with siRNA targeting a negative control (siControl), Orc1 as a positive control (siOrc1),
945 or Orc6 (siOrc6) for 42 h. (**B**) Western blot analysis of whole-cell fractions from cells
946 treated with siRNA against a negative control (siControl), Orc1 (siOrc1), and Orc6
947 (siOrc6), using antibodies against Orc6, Orc1, and histone H3. Molecular weight
948 markers (kDa) are indicated on the right. (**C**) Single-cell plot analysis of Mcm2 in
949 hTERT-RPE1 cells treated with siRNA (siControl, siOrc1, or siOrc6). siRNA-treated
950 cells were fixed using the pre-extraction method and stained with Hoechst and anti-
951 Mcm2 antibody. Cells with high Mcm2 levels (> half the maximum Mcm2 value,
952 excluding the 4 highest values among 450 cells) and low DNA content (Hoechst <
953 1.125) are marked cyan. n = 450 (number of cells examined in each panel). **(D)**
954 Percentages of cyan-marked cells (high MCM) among G1-phase cells (Hoechst <
955 1.125) based on (**C**). Columns and error bars represent the mean and standard error of
956 the mean of three independent experiments. Statistical difference (p = 0.004) was
957 determined using a one-sided t-test. (**E**) Timing diagram for siRNA treatment and
958 MG132 addition. hTERT-RPE1 cells were treated with siRNA. After 18 h of siRNA
959 treatment, MG132 was added at 312 nM for an additional 24 h, with continued siRNA
960 treatment. (**F**) Single-cell plot analysis of Mcm2 in hTERT-RPE1 cells treated with
961 siRNA (siControl, siOrc1, or siOrc6), with MG132 addition. Cells with high Mcm2
962 levels ($\log_2$[Mcm2] > −1.5) and high DNA content (Hoechst > 1.8) are marked magenta.
963 n = 450 (number of cells examined in each panel). Another experiment with different
964 siRNA is shown in Fig. S6A. (**G**) Percentage of magenta-marked cells ($\log_2$[Mcm2] >
965 −1.5 and Hoechst > 1.8) among G2-phase cells (Hoechst >1.8) based on (**F**). Columns
966 and error bars represent the mean and standard error of the mean of four independent
967 experimental results. Statistical differences (p = 0.0006) were determined using a one-
968 sided t-test. (**H**) Western blot analysis of whole-cell lysates from hTERT-RPE1 cells

969 treated with siControl or siCdc6), using antibodies against Cdc6 and GAPDH.
970 Molecular weight markers (kDa) are indicated on the right. (**I**) Single-cell plot analysis
971 of chromatin-bound Mcm2 in hTERT-RPE1 cells treated with siControl or siCdc6. After
972 MG132 treatment, cells were fixed using the pre-extraction method and stained with
973 Hoechst and anti-Mcm2 antibody. Cells with high MCM levels ($\log_2$[Mcm2] > −1.5)
974 and high DNA content (Hoechst > 1.8) are marked magenta. n = 450 (number of cells
975 examined in each panel). Another experiment with a different siRNA is shown in Fig.
976 S6B. (**J**) Percentage of magenta-marked cells ($\log_2$[Mcm2] > −1.5 and Hoechst > 1.8)
977 among G2-phase cells (Hoechst > 1.8) based on (**I**). Columns and error bars represent
978 the mean and standard error of the mean of three independent experiments. Statistical
979 difference (p = 0.001) was determined using a one-sided t-test.
980
981 **Figure 8. Schematic diagram of Orc6 behavior**
982 (**A**) Normal proteasome activity: After DNA replication, Cdt1 and Orc1 are degraded by
983 proteasome activity, and Orc6 dissociates from chromatin, preventing MCM reloading.
984 Cells enter mitosis and produce normal diploid cells. Orc2–5 represents a complex of
985 Orc2, Orc3, Orc4, and Orc5. (**B**) Loss of proteasome activity: Orc6, Orc1, Cdt1, and
986 MCM are reloaded onto chromatin without mitosis, allowing cells to re-enter the
987 replication phase as tetraploid cells.
988

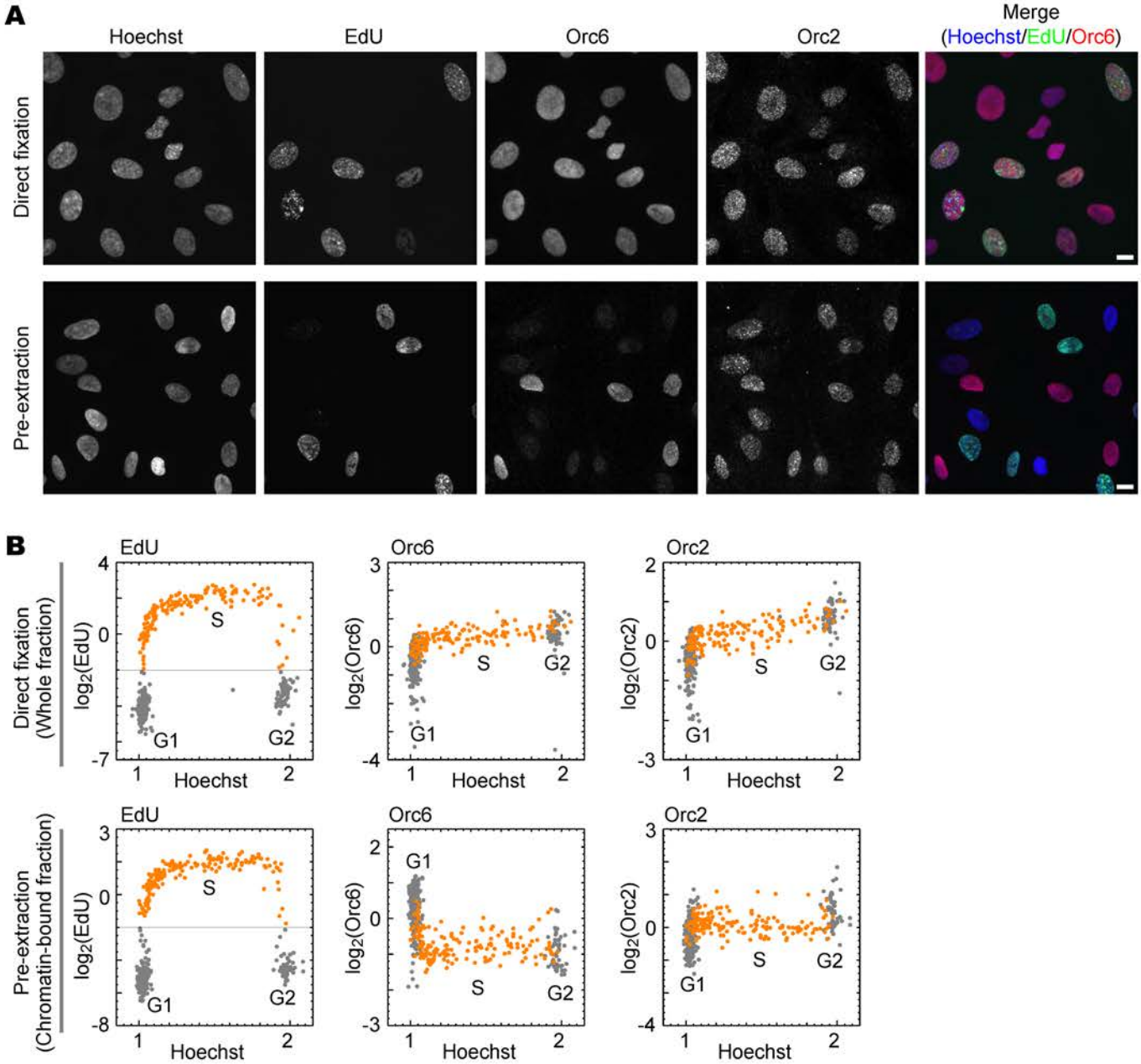
A
Hoechst
EdU
Orc6
Orc2
Merge
(Hoechst/EdU/Orc6)
Direct fixation
Pre-extraction
B
EdU
Orc6
Orc2
Direct fixation
(Whole fraction)
Pre-extraction
(Chromatin-bound fraction)
log2(EdU)
log2(Orc6)
log2(Orc2)
Hoechst
G1
S
G2

Figure 1

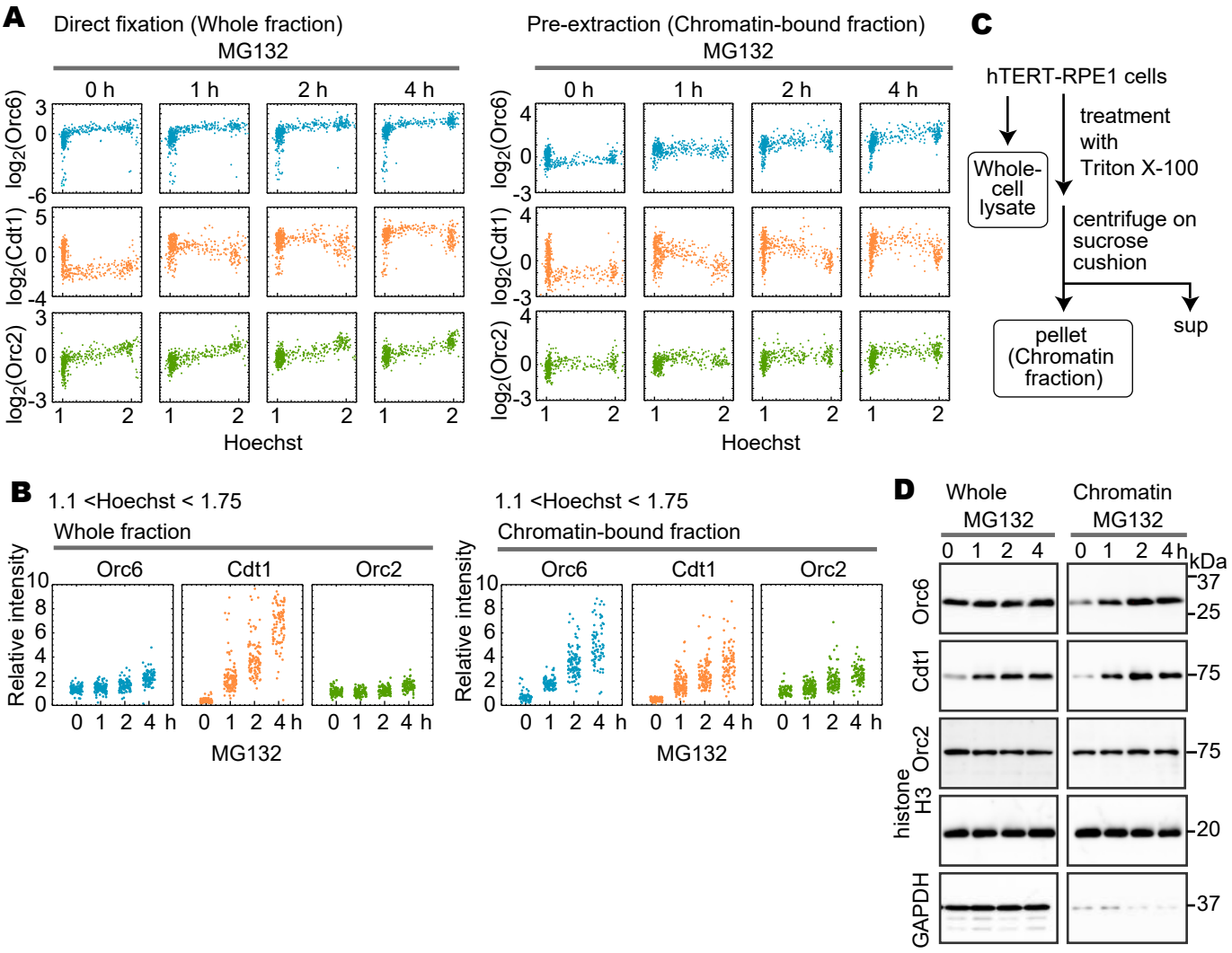
A
Direct fixation (Whole fraction)
MG132
0 h
1 h
2 h
4 h
log2(Orc6)
log2(Cdt1)
log2(Orc2)
Hoechst
Pre-extraction (Chromatin-bound fraction)
MG132
C
hTERT-RPE1 cells
Whole-cell lysate
treatment with Triton X-100
centrifuge on sucrose cushion
pellet (Chromatin fraction)
sup
B
1.1 <Hoechst < 1.75
Whole fraction
Orc6
Cdt1
Orc2
Relative intensity
MG132
1.1 <Hoechst < 1.75
Chromatin-bound fraction
D
Whole
MG132
Chromatin
MG132
kDa
Orc6
Cdt1
Orc2
histone H3
GAPDH
37
25
75
75
20
37

Figure 2

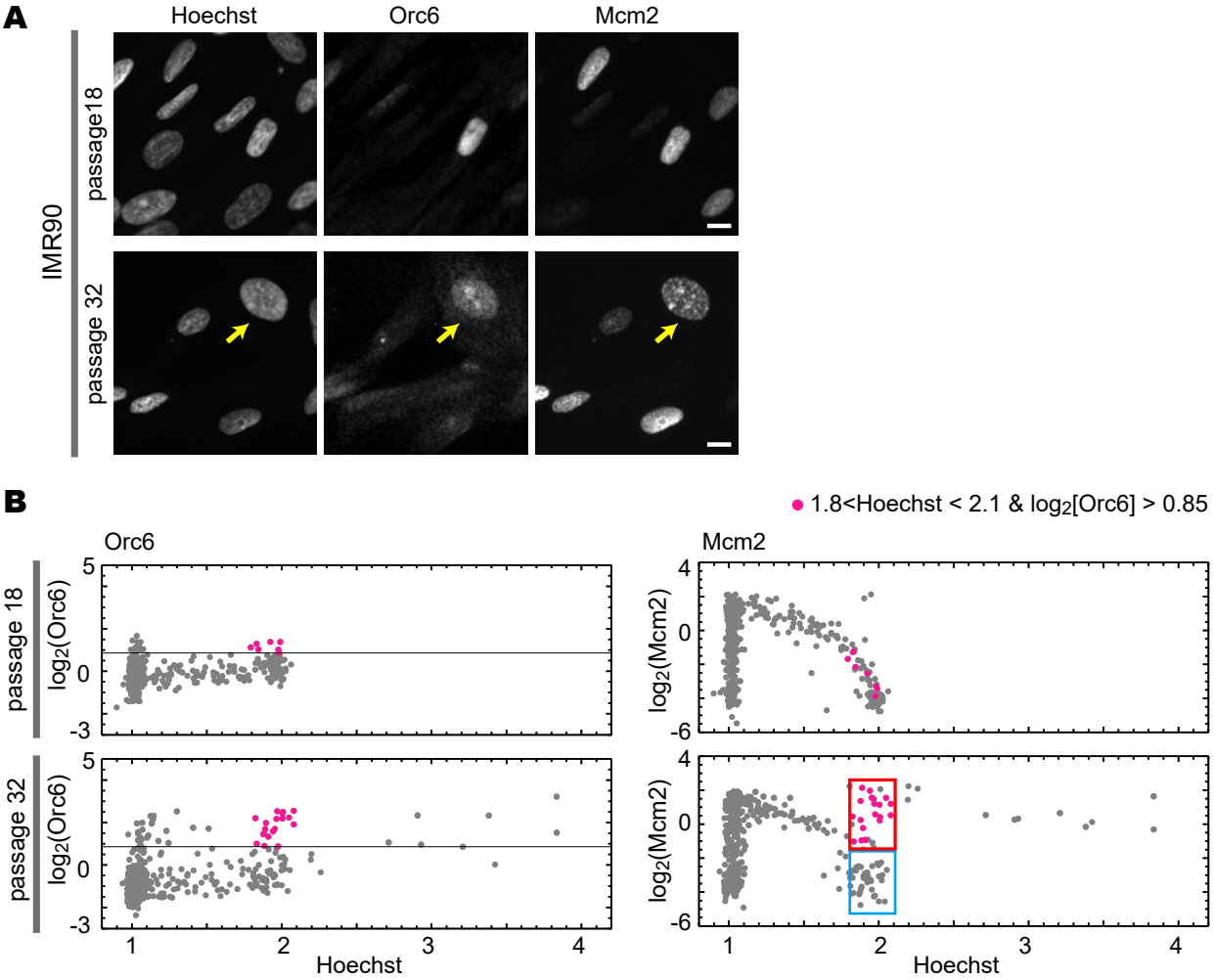
A
Hoechst
Orc6
Mcm2
IMR90
passage18
passage 32
B
1.8<Hoechst < 2.1 & log2[Orc6] > 0.85
Orc6
Mcm2
passage 18
passage 32
log2(Orc6)
log2(Mcm2)
Hoechst

Figure 3

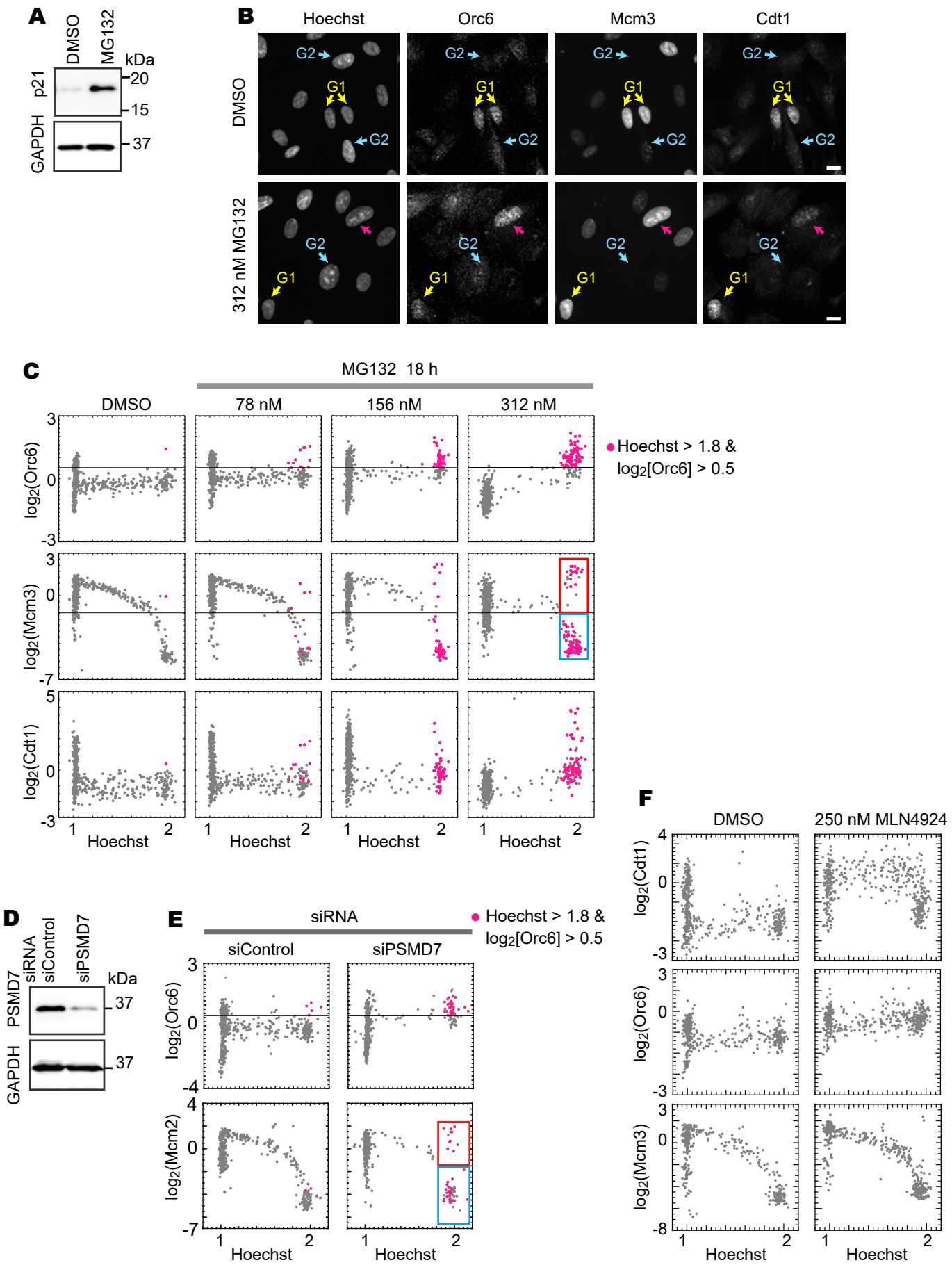
A
DMSO
MG132
kDa
p21
20
15
GAPDH
37
B
Hoechst
Orc6
Mcm3
Cdt1
DMSO
312 nM MG132
G2
G1
C
MG132 18 h
DMSO
78 nM
156 nM
312 nM
log2(Orc6)
log2(Mcm3)
log2(Cdt1)
Hoechst
Hoechst > 1.8 &
log2[Orc6] > 0.5
D
siRNA
siControl
siPSMD7
PSMD7
E
siRNA
log2(Mcm2)
F
250 nM MLN4924

Figure 4

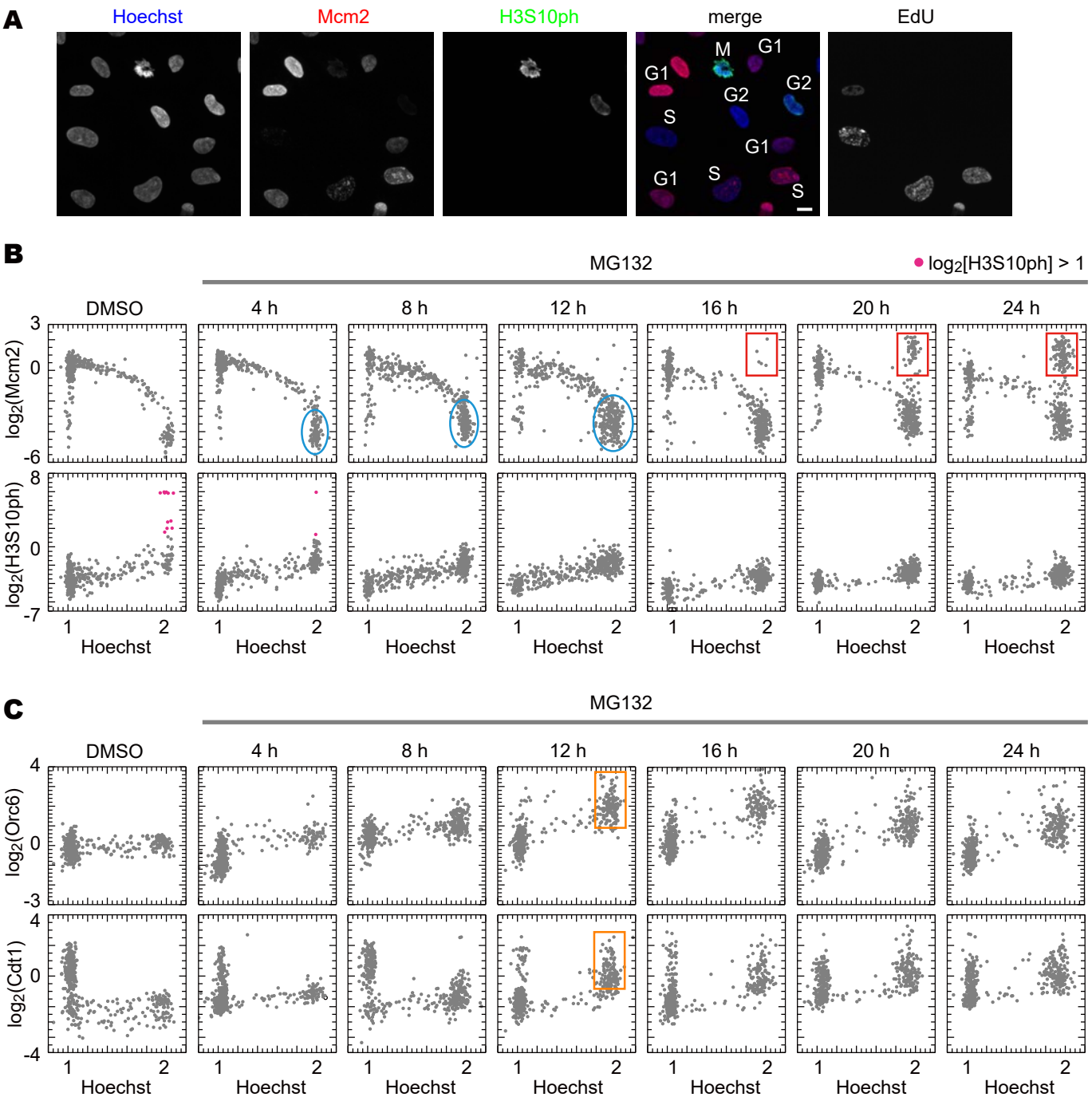
A
Hoechst
Mcm2
H3S10ph
merge
EdU
M
G1
G2
S
B
MG132
log2[H3S10ph] > 1
DMSO
4 h
8 h
12 h
16 h
20 h
24 h
log2(Mcm2)
log2(H3S10ph)
Hoechst
C
log2(Orc6)
log2(Cdt1)

Figure 5

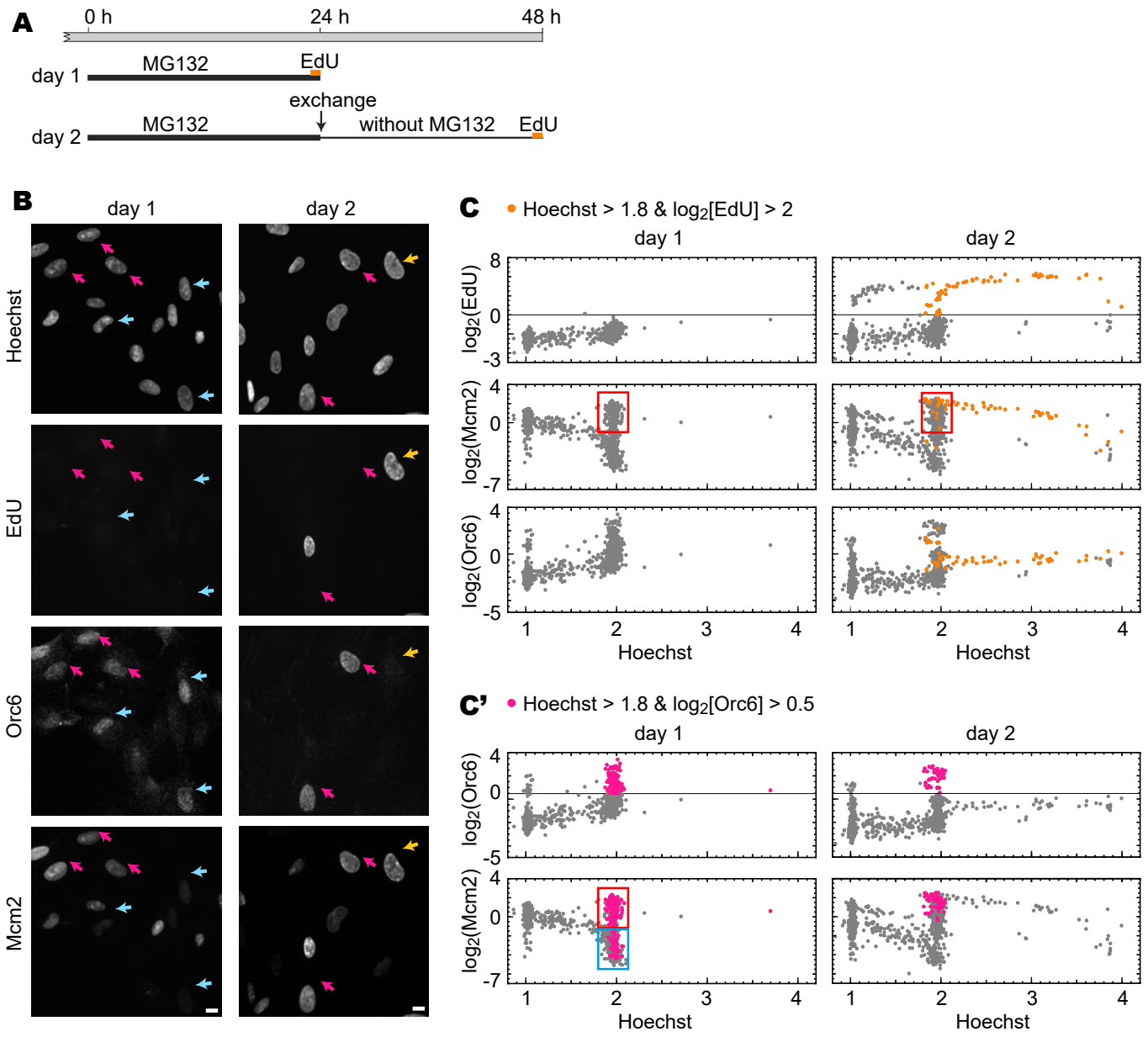
A
0 h
24 h
48 h
day 1
MG132
EdU
exchange
day 2
MG132
without MG132
EdU
B
day 1
day 2
Hoechst
EdU
Orc6
Mcm2
C
Hoechst > 1.8 & log2[EdU] > 2
day 1
day 2
log2(EdU)
log2(Mcm2)
log2(Orc6)
Hoechst
C'
Hoechst > 1.8 & log2[Orc6] > 0.5
day 1
day 2
log2(Orc6)
log2(Mcm2)
Hoechst

Figure 6

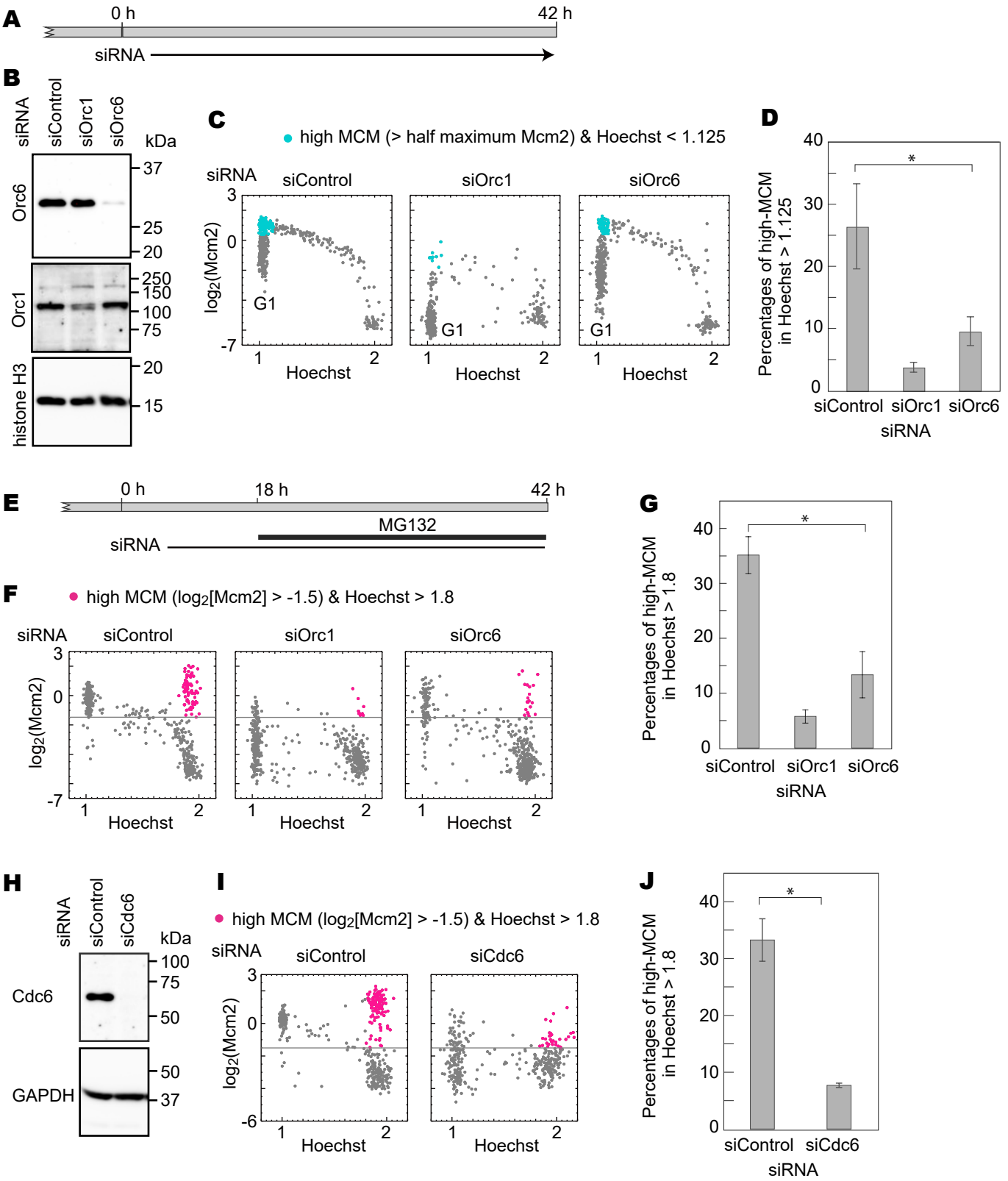
A
0 h
42 h
siRNA
B
siRNA
siControl
siOrc1
siOrc6
kDa
Orc6
Orc1
histone H3
37
25
20
250
150
100
75
20
15
C
high MCM (> half maximum Mcm2) & Hoechst < 1.125
siRNA
siControl
siOrc1
siOrc6
log2(Mcm2)
G1
Hoechst
D
Percentages of high-MCM in Hoechst > 1.125
siRNA
E
0 h
18 h
42 h
MG132
siRNA
F
high MCM (log2[Mcm2] > -1.5) & Hoechst > 1.8
G
Percentages of high-MCM in Hoechst > 1.8
H
siCdc6
Cdc6
GAPDH
I
J

Figure 7

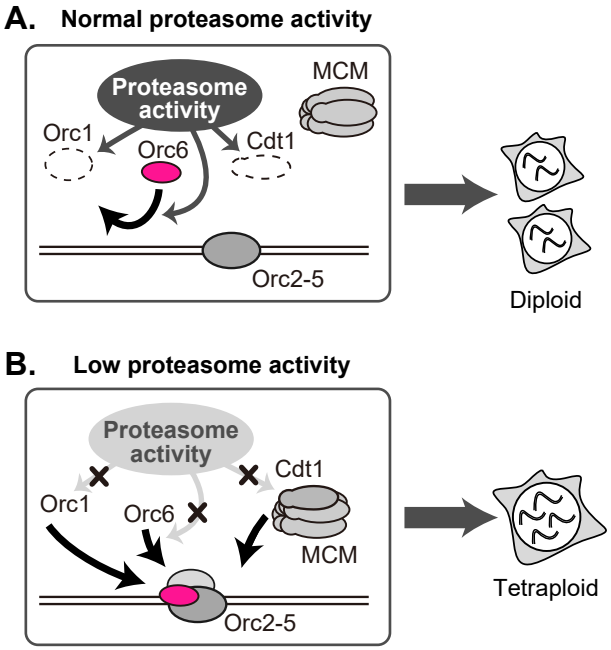
A.
Normal proteasome activity
Proteasome activity
MCM
Orc1
Orc6
Cdt1
Orc2-5
Diploid
B.
Low proteasome activity
Proteasome activity
Cdt1
Orc1
Orc6
MCM
Orc2-5
Tetraploid

Figure 8

Supplemental Figures

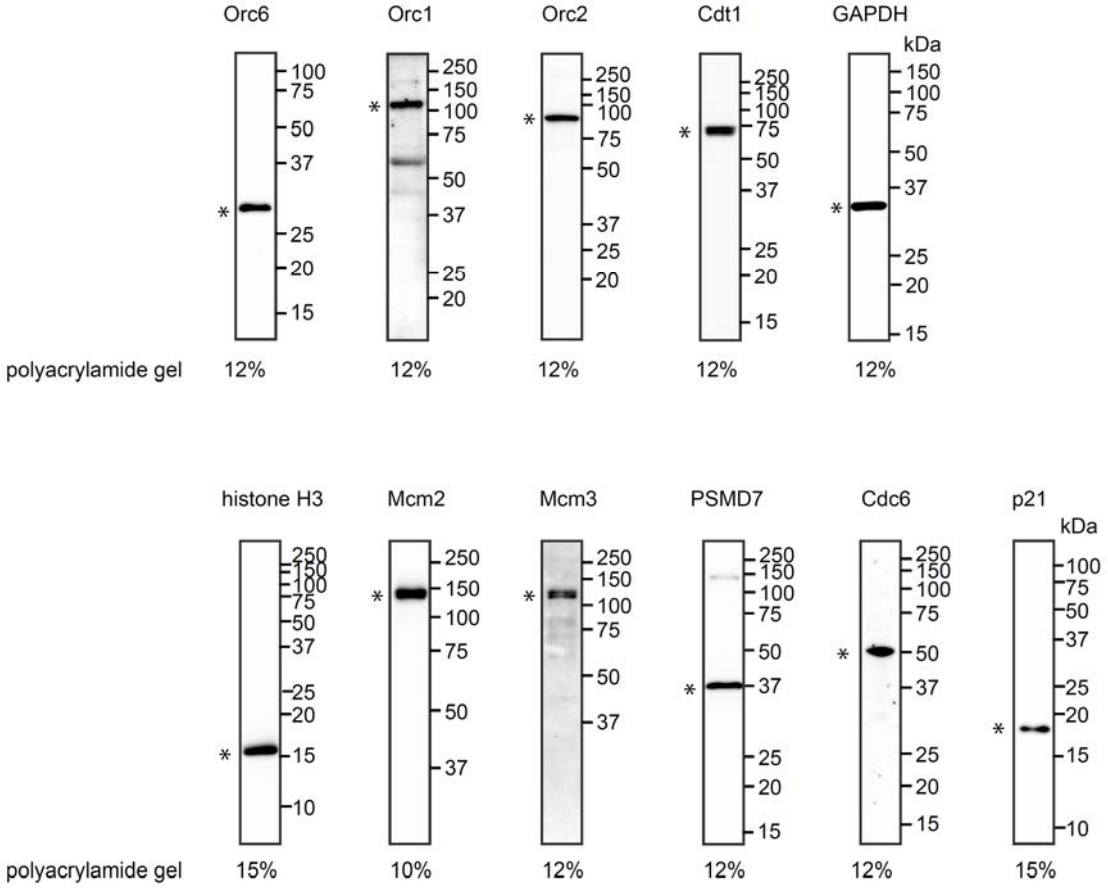

Figure S1. Validation of antibodies used in this study

Western blot analysis of whole-cell lysates from hTERT-RPE1 cells using antibodies against Orc6, Orc1, Orc2, Cdt1, GAPDH, histone H3, Mcm2, Mcm3, PSMD7, Cdc6, and p21. Molecular weight markers (kDa) are indicated on the right of each blot. The percentage of polyacrylamide gel used is shown below each blot. Asterisks (*) indicate the proteins of interest detected at their expected molecular weights.

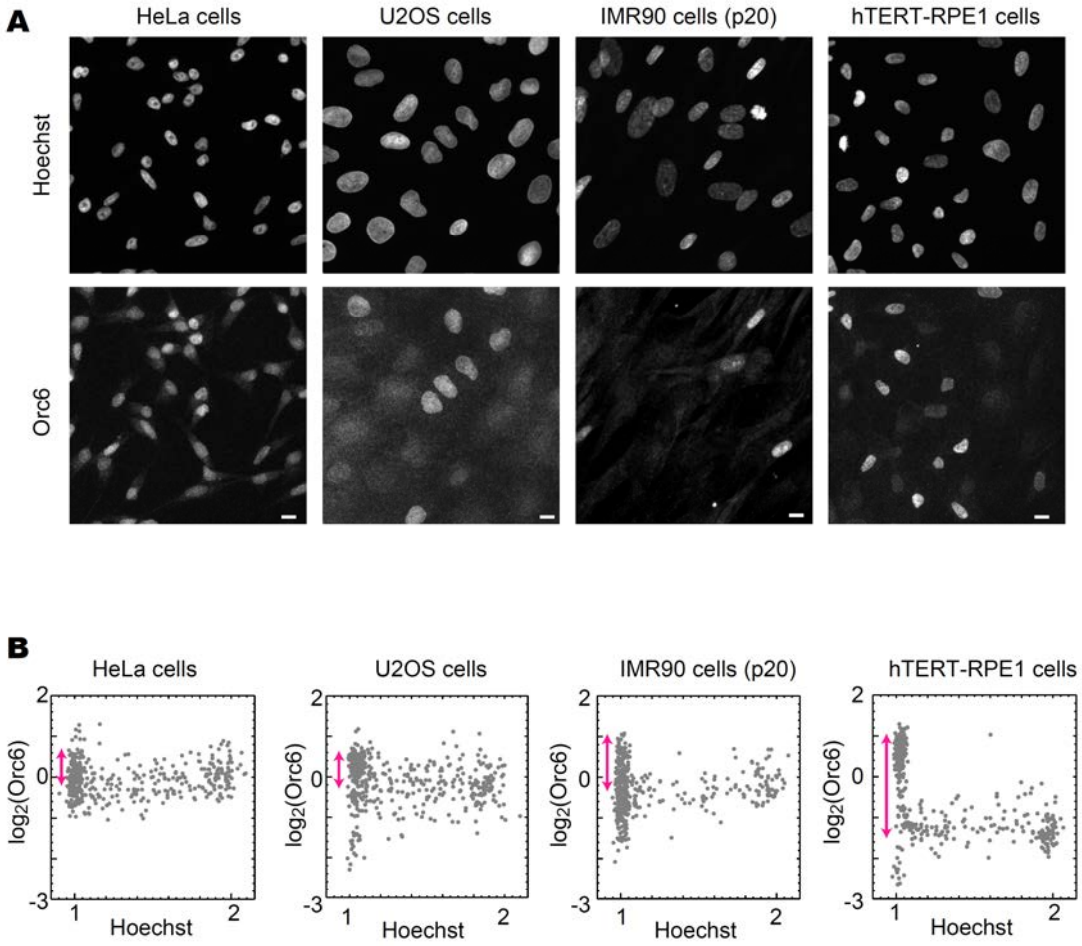

Figure S2. Behaviors of chromatin-bound Orc6 during the cell cycle in HeLa, U2OS, IMR90, and hTERT-RPE1 cells

(**A**) Representative fluorescence images of Hoechst and Orc6 staining in HeLa (left), U2OS (second left), IMR90 (second right), and hTERT-RPE1 (right) cells. Cells were fixed using the pre-extraction method and stained with Hoechst and anti-Orc6 antibody. The method of pre-extraction reproducibly makes the nuclei of HeLa cells smaller, but not in U2OS cells, for unknown reasons. Scale bars, 10 µm. (**B**) Single-cell plot analysis based on the images in (**A**). Each dot represents the intensities of Orc6 in an individual cell plotted against the Hoechst intensities. Magenta arrows show the difference in Orc6 levels from the 10th highest intensity in G1 (Hoechst < 1.1) to the Orc6 average intensity in early S-phase (1.15 < Hoechst < 1.4). n = 450 (number of cells examined in each panel).

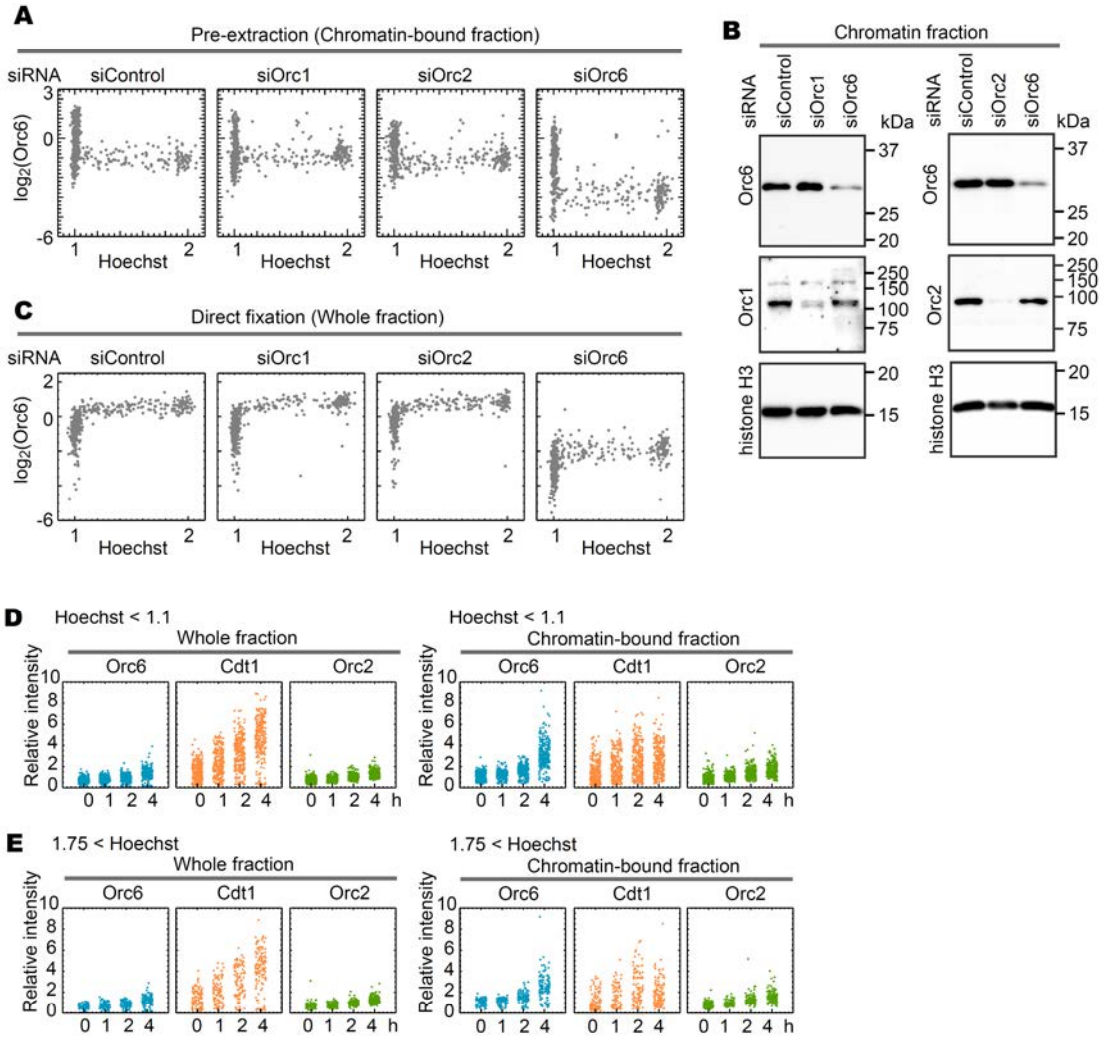

Figure S3. Chromatin binding of Orc6 is independent of the presence of Orc1 and Orc2

(**A**) Single-cell plot analysis of Orc6 in hTERT-RPE1 cells treated for 24 h with siRNA against a negative control (siControl), Orc1 (siOrc1), Orc2 (siOrc2), and Orc6 (siOrc6), and fixed using the pre-extraction method to obtain the chromatin-bound fraction. The cells were stained with Hoechst and anti-Orc6 antibody. n = 450 (number of cells examined in each panel). (**B**) Western blot analysis using antibodies against Orc6, Orc1, Orc2, and histone H3. hTERT-RPE1 cells were treated for 24 h with siRNA (siControl, siOrc1, siOrc2, or siOrc6). Chromatin fractions were prepared from these cells using the sucrose cushion fractionation as described in Methods and subjected to western blot analyses. Histone H3 is a loading control. Molecular weight markers (kDa) are indicated on the right. (**C**) Single-cell plot analysis of Orc6 in hTERT-RPE1 cells treated for 24 h

with siRNA against a negative control (siControl), Orc1 (siOrc1), Orc2 (siOrc2), and Orc6 (siOrc6), and directly fixed to obtain the chromatin-bound fraction. The cells were stained with Hoechst and anti-Orc6 antibody. n = 450 (number of cells examined in each panel). (**D, E**) Orc6, Cdt1, and Orc2 levels in G1- **(D)** and G2-phases cells **(E)**. Cells corresponding to G1-phase (Hoechst < 1.1) or G2-phase (1.75 < Hoechst) are selected from (Fig. 2A), and their fluorescence intensities were plotted. The average intensity in MG132-untreated cells (0 h) was defined as 1.

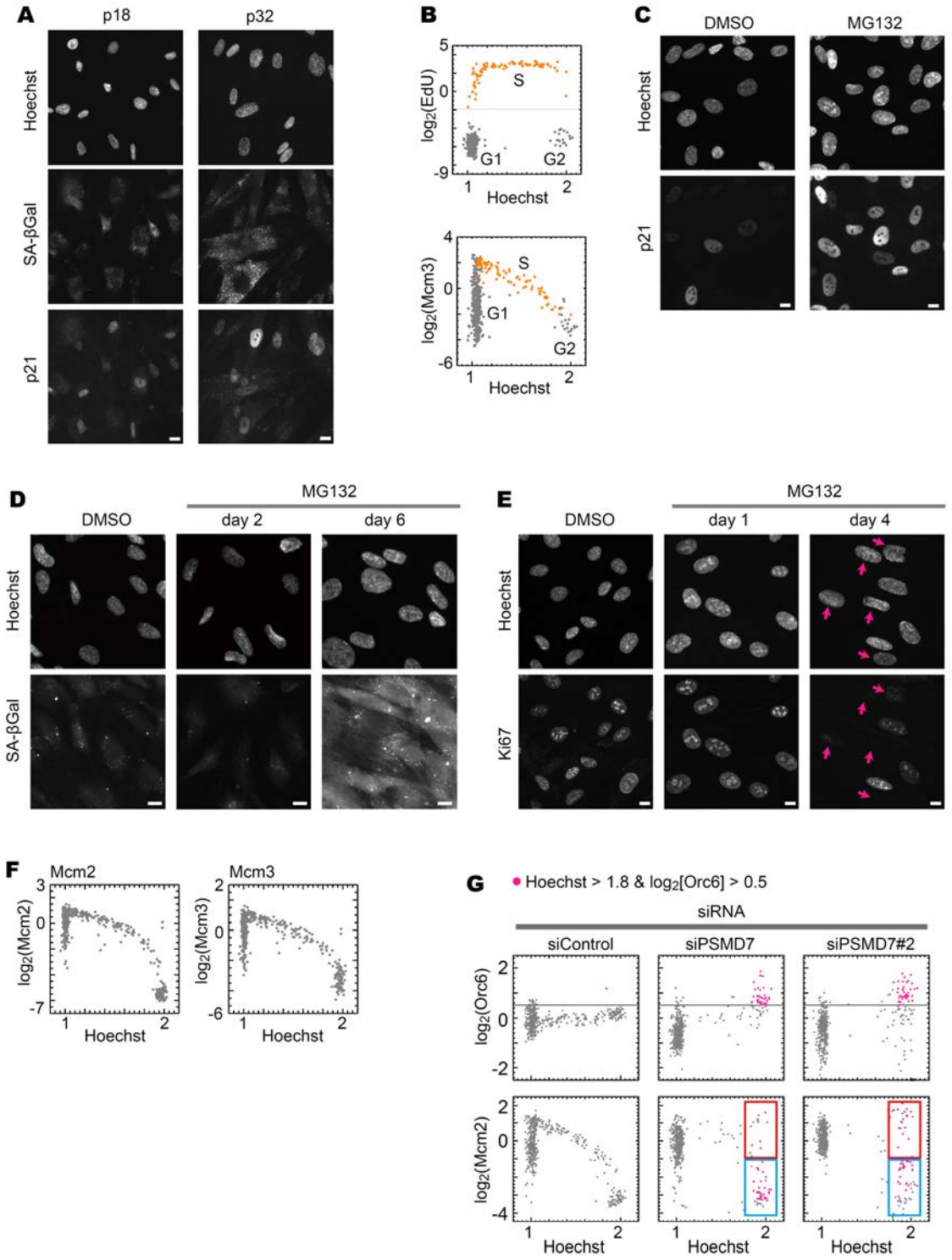

Figure S4. Effect of MG132 treatment on hTERT-RPE1 cells

(**A**) Representative fluorescence images of Hoechst, SA-βGal and p21 staining in IMR90 cells (passage numbers 18 and 32). Cells were fixed using the direct fixation

method. **(B)** Single-cell plot analysis of IMR90 cells (passage 18) co-immunostained with EdU and Mcm3. Cells were treated with EdU for 30 min prior to collection and then fixed using the pre-extraction method. Each dot represents the intensities of EdU and Mcm3 in an individual cell, plotted against Hoechst 33342 intensities. Orange dots represent S-phase cells based on EdU intensities (log2(EdU) > –2). The number of cells examined in each panel is 450. (**C**) Representative fluorescence images of Hoechst and p21 staining in hTERT-RPE1 cells treated with DMSO or 312 nM MG132 on day 1. Cells were fixed using the direct fixation method. **(D)** Representative images of Hoechst and SA-βGal staining in cells treated with DMSO or 312 MG132 on day 2 and on day 6. Before the direct fixation method for Hoechst staining, cells were incubated with the reagent according to the manual. **(E)** Representative images of Hoechst and Ki67 staining in cells treated with DMSO or 312 nM MG132 on day 1 and on day 4. Cells were fixed using the direct fixation method. Red arrows indicate Ki67 negative cells. **(F)** Single-cell plot analysis of hTERT-RPE1 cells co-immunostained with Mcm2 and Mcm3. The number of cells examined in each panel is 450. **(G)** Single-cell plot analysis of Orc6 and Mcm2 in hTERT-RPE1 cells treated with negative control-siRNA (siControl) or two types of PSMD7-siRNA (siPSMD7). Cell conditions and immunostaining methods were the same as in Fig.4E. Scale bars, 10 μm.

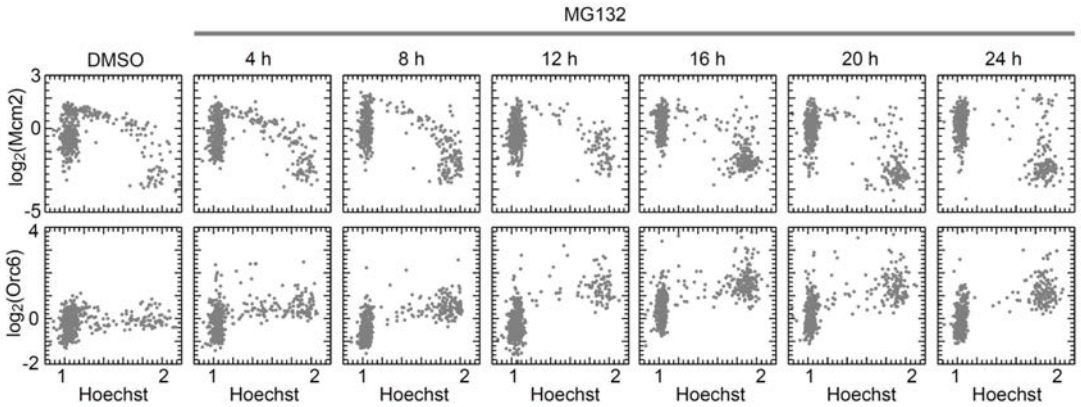

Figure S5. Time course from MG132 treatment to the appearance of cells with high chromatin-bound MCM and Orc6

Single-cell plot analysis of Mcm2 (top) and Orc6 (bottom) in cells treated with DMSO or 312 nM MG132 for the indicated durations. The same conditions but different combinations are shown in Fig. 5B, 5C. n = 450 (number of cells examined in each panel).

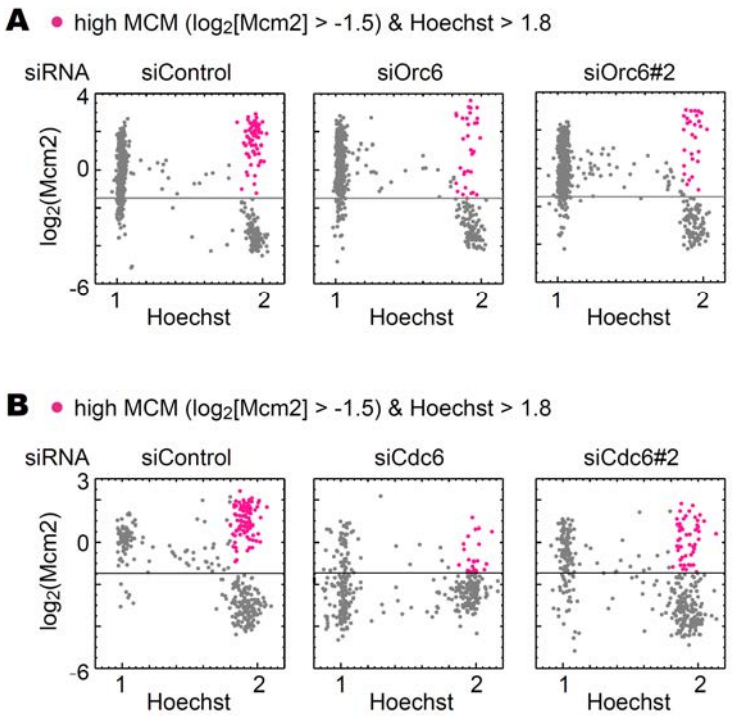

Figure S6. Single-cell plot analysis in siRNA-treated cells

(A, B) Single-cell plot analysis of Mcm2 in cells treated with siOrc6 and siOrc6#2 (**A**), and siCdc6 and siCdc6#2 **(B)**. Cells with high Mcm2 levels ($\log_2$[Mcm2] > −1.5) and high DNA content (Hoechst > 1.8) are marked magenta. n = 450 (number of cells examined in each panel).

Fig. 2D

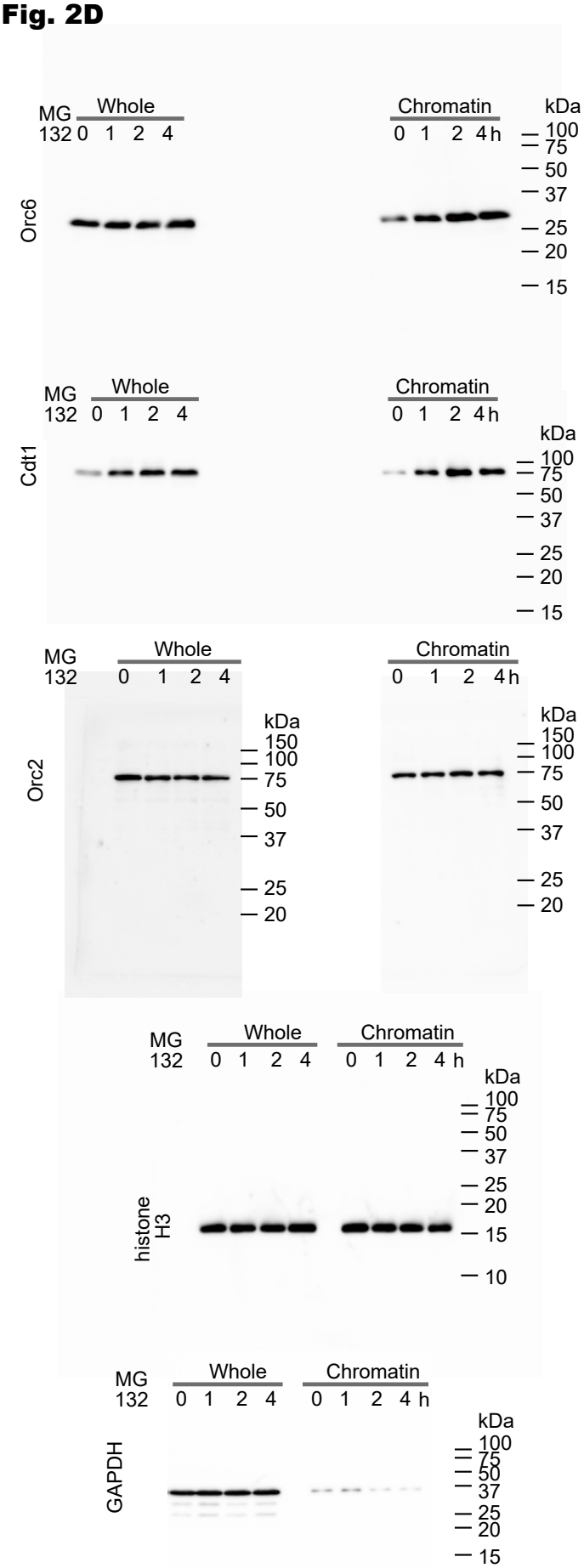

Fig. 4A

Fig. 4D

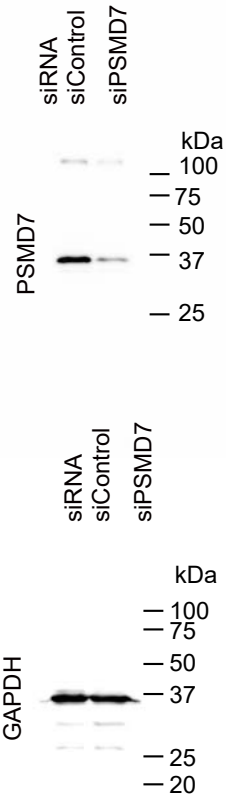

Western blot transparency_1

Fig. 7B

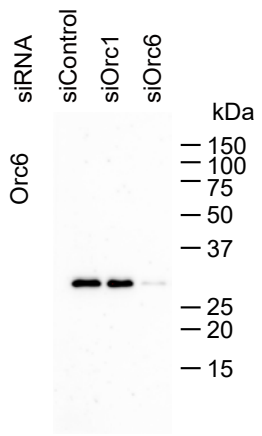

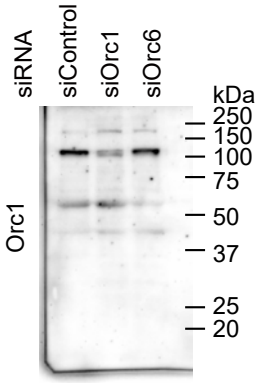

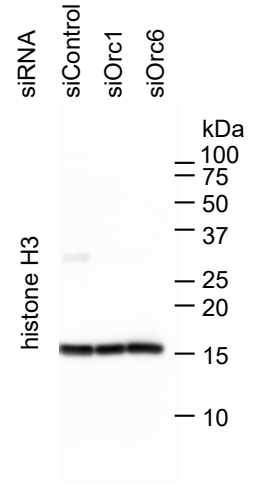

Fig. 7H

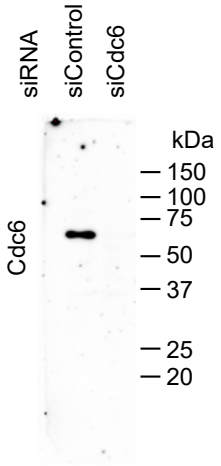

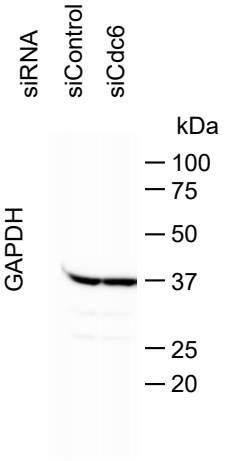

Western blot transparency_2